USDOT Region V Regional University Transportation Center Final Report

NEXTRANS Project No. 107PUY2.1

Developing Operational and Policy Insights into Next Generation Vehicle Needs Based on an Integrated Understanding of the Transportation and Energy System of Systems

By

Shubham Agrawal
Ph.D. student, School of Civil Engineering
Purdue University
shubham@purdue.edu

and

Xiaohui Liu
Ph.D. student, School of Chemical Engineering
Purdue University
liu668@purdue.edu

and

Joseph F. Pekny
Professor of Chemical Engineering
Purdue University
pekny@purdue.edu

and

Srinivas Peeta
Professor of Civil Engineering
Purdue University
peeta@purdue.edu

and

J. Eric Dietz
Professor of Computer and Information Technology
Purdue University
jedietz@purdue.edu

and

Mohammad Miralinaghi
Ph.D. student, School of Civil Engineering
Purdue University
smiralin@purdue.edu

DISCLAIMER

Funding for this research was provided by the NEXTRANS Center, Purdue University under Grant No. DTRT12-G-UTC05 of the U.S. Department of Transportation, Office of the Assistant Secretary for Research and Technology (OST-R), University Transportation Centers Program. The contents of this report reflect the views of the authors, who are responsible for the facts and the accuracy of the information presented herein. This document is disseminated under the sponsorship of the Department of Transportation, University Transportation Centers Program, in the interest of information exchange. The U.S. Government assumes no liability for the contents or use thereof.

USDOT Region V Regional University Transportation Center Final Report

TECHNICAL SUMMARY

NEXTRANS Project No. 107PUY2.1 Final Report, 31st July 2016

Title

Developing Operational and Policy Insights into Next Generation Vehicle Needs Based on an Integrated Understanding of the Transportation and Energy System of Systems

Introduction

Electric vehicles (EVs) have received considerable attention in the recent past with the promise of achieving reduced petroleum dependency, enhanced energy efficiency, and improved environmental sustainability. EVs, especially battery electric vehicles (BEVs), have different characteristics and concerns as compared to internal combustion engine vehicles (ICEVs) such as range limitation, range anxiety, long battery recharging time, lower fuel efficient speed, and recuperation of energy lost during the deceleration phase if equipped with regenerative braking system (RBS). Hence, it is expected that BEV and ICEV drivers will have different travel behaviors, e.g. route choice. With increasing the market penetration of BEVs, this difference in travel behavior will have implications on the network performance, especially in terms of system travel time and overall energy consumption. This study develops a multi-class dynamic user equilibrium (MCDUE) model to evaluate the traffic network performance under equilibrium conditions for mixed traffic flow with BEVs and ICEVs by accounting for the difference in their route choice behavior.

Further, the driving range of an EV decreases due to battery degradation with use and time. This can make EVs less attractive for consumers as battery replacement is expensive. This study develops a multi-paradigm modeling framework integrating microscopic traffic simulation model, EV energy consumption model, battery circuit model, and semi-empirical battery degradation model to study the impacts of EV travel patterns on battery lifespan.

Findings

The results from MCDUE model provide useful insights related to the BEV route choice behavior and its impact on network performance. As the battery state-of-charge consumption of BEVs is lower at slower speeds, BEVs tend to select routes with lower speeds to reduce electricity costs and avoid range anxiety. Moreover, the electricity regeneration during braking due to RBS makes it economical for BEVs to select routes with stop-and-go traffic conditions. Such potential unconventional route choice behavior of BEVs can reduce congestion on routes with higher speeds, e.g. freeways, while increasing congestion on routes with lower speeds, e.g. arterial routes. This can potentially lead to improvement in network performance and move the traffic network towards system optimal conditions in terms of travel time. The results also

indicate that with increase in traffic congestion, the route choice behavior of EVs become similar to ICEVs as the difference in speed between freeways and arterial routes decreases.

This study quantifies the impacts of temperature, vehicle travel patterns, and driving behavior on battery lifespan for a large EV population. The results illustrate that at lower temperatures, the variation in battery lifespans of a large population of EVs is higher due to differences in vehicle travel patterns and driving behavior. The battery lifespan decreases as the average daily distance traveled increases. The results also indicate that the battery lifespan is lower for the drivers with high speed variation during driving. The variation in battery lifespan decreases with increase in temperature.

Recommendations

The research insights of this project can be leveraged by traffic operators, energy operators, vehicle owners, policymakers and vehicle manufacturers. First, traffic operators need to incorporate the difference in route choice behavior of BEVs and ICEVs in devising control strategies to enhance the traffic network performance without exclusively using just monetary instruments like tolling or congestion pricing, at least under mixed traffic environments. Second, the insights related to energy consumption can aid energy operators to plan for infrastructure investments to support the increasing market penetration of electric vehicles. Third, vehicle owners should assess the lifetime cost of EV ownership including maintenance cost, insurance cost and battery resale value, based on their travel needs and geographic location. Finally, policymakers and vehicle manufacturers should factor regional temperature conditions in designing strategies, e.g. tax credits and battery warranty, to promote EV adoption. Since the impacts of vehicle travel patterns and driving behavior are considerable at lower temperatures, these need to be factored by vehicle manufacturers in designing of warranty strategies for colder regions.

ACKNOWLEDGEMENT

The authors would like to thank the NEXTRANS Center, the USDOT Region V Regional University Transportation Center at Purdue University, for supporting this research.

TABLE OF CONTENTS

LIST OF FIGURES

LIST OF TABLES

CHAPTER 1. INTRODUCTION

1.1 Background and motivation

The transportation sector is an important component of energy consumption. It accounts for about 70% of the total oil consumption in the U.S. (U.S. EIA, 2012; U.S. EPA, 2015). Internal combustion engine vehicles (ICEVs) use liquid fossil fuels as their energy sources, and have become the largest contributors to urban air pollution (Funk and Rabl, 1999). In 2013, greenhouse gas emissions from transportation sector accounted for about 27% of total U.S. greenhouse gas emissions, making it the second largest contributor of greenhouse gas emissions in the U.S. after the electricity sector (U.S. EPA, 2015). Electric vehicles have received considerable attention in the recent past with the promise of achieving reduced petroleum dependency, enhanced energy efficiency, and improved environmental sustainability. An electric vehicle (EV) uses a battery-powered electric motor for propulsion unlike an ICEV which is powered by burning gasoline or diesel. Although the environmental sustainability of EVs is debated for the source of electricity generated for recharging the EV's battery, they have a clear advantage over ICEVs due to their energy efficiency. Since electricity can be generated from renewable energy, EVs have the potential to significantly reduce emissions from transportation sectors as the electricity fuel mix evolves (EPRI, 2007; Wang, 1999; Weiller, 2011). According to the U.S. Department of Energy (USDOE, 2014), it is estimated that only about 17–21% of the energy stored in the gas tank of an ICEV is converted to power at the wheels because for example, the combustion engine alone loses 62.4% of the energy from fuel as heat. By contrast, EVs convert about 59–62% of the electrical energy from the grid to power at the wheels. EVs can be equipped with regenerative braking system that can further enhance overall fuel efficiency and reduce emissions (Clarke et al., 2010).

However, the greater adoption of EV still faces several substantial challenges. These include range anxiety (that is, the fear of running out of battery charge before completing the trip) (Tate et al., 2008), long battery recharging time (Morrow et al., 2008),

scarce availability of charging infrastructure (Lin and Greene, 2011; Miralinaghi et al., 2017, 2016; Pearre et al., 2011), the potential impact on power grid stability (Kang and Recker, 2009), higher vehicle prices (Rezvani et al., 2015), and concerns about battery such as reduction in lifespan due to degradation and resale value for second use (Neubauer et al., 2012; Saxena et al., 2015). Thus, a realistic framework to analyze the impacts of EVs based on an integrated understanding of the transportation and energy system of systems is essential for developing operational and policy insights.

1.2 Research objectivess

The research objectives are the following:

- Develop a multi-class dynamic user equilibrium (MCDUE) model to evaluate the network performance under equilibrium conditions for mixed traffic flow with EVs and ICEVs by accounting for the difference in their route choice behavior.
- Develop a multi-paradigm modeling framework to quantify EV battery lifespan for a large population of EVs by integrating microscopic traffic simulation model, EV energy consumption model, battery circuit model, and semi-empirical battery degradation model.

1.3 Organization of the research

The remainder of the report is organized as follows. CHAPTER 2 presents the conceptual foundation for the proposed study and reviews related literature. CHAPTER 3 presents a framework to study the routing aspects of EV drivers and their effects on the network performance. CHAPTER 4 presents a multi-paradigm modeling framework to quantify the impacts of EV travel patterns on battery lifespan. CHAPTER 5 summarizes the research findings and insights, and discusses future research directions.

CHAPTER 2. CONCEPTUAL FOUNDATION AND LITERATURE REVIEW

This chapter introduces the conceptual foundation of the study and literature review on existing tools for quantifying the impacts of EVs on transportation network performance, and the impacts of EV travel patterns on battery lifespan.

2.1 Electric vehicle characteristics

There are two main types of EVs in the market: plug-in hybrid electric vehicle (PHEV) and battery electric vehicle (BEV). PHEVs are equipped with both internal combustion engine and electric motor, and BEVs are equipped with only the electric motor. As a PHEV uses two drive-trains, typically its operating cost is higher than that of a BEV which uses single drive-train. There are unique characteristics currently associated with BEVs, including limited battery capacity and long recharging time that can be limiting for travel compared to ICEVs. Given the current battery technologies, a BEV typically has a driving range of around 80 – 100 miles with a full charge, depending on the vehicle type and battery size. Some premium BEVs, such Tesla Model S, have a higher range of about 250 – 350 miles with the advancement of battery technology which is expected to improve further; however, they are significantly more expensive compared to typical EVs. The limited driving range of BEVs imposes an issue, known as the range anxiety, that is, the driver concerns that the vehicle will run out of battery power before reaching the destination (Tate et al., 2008). This issue is especially limiting for long trips where the travel distance is close to or beyond the driving range (Mock et al., 2010; Yu et al., 2011). This study focuses on BEVs rather than PHEVs as the purpose of this study is to capture range anxiety which is not applicable to PHEVs. A PHEV is similar to a BEV when operating on battery (if range anxiety is not a concern) and an ICEV when operating on gasoline or diesel.

Typically, a BEV spends 6-8 hours (slow charging) to get fully charged, depending on the electrical charging equipment, charging schemes, and battery capacity (Botsford and

Szczepanek, 2009). Fast charging technology is available, with 10 minutes charging for a range up to 100 miles. However, it requires special equipment in the power connector and is sparsely deployed in the public infrastructure. Even the “quick charge” facility available at public charging stations can take around 30 minutes to charge the battery up to 80% (USDOE, 2016). Furthermore, fast charging, including quick charging, can deteriorate the battery health and is not advisable on a regular basis (Rezvanizaniani et al., 2014). Another alternative to en route charging for long distance travel is battery swapping stations (BSS) where a depleted battery pack is quickly swapped with a recharged one. The success of BSS requires car manufacturers to follow certain battery standards, and even then can entail battery stock problem, especially in urban areas. These technological and logistical challenges make BSS impractical to implement (Senart et al., 2010). Therefore, BEV drivers currently, and in the near future, are expected to charge their vehicles through home-based overnight charging or workplace-based charging mechanisms most of the time.

2.2 Electric vehicle energy consumption models

In the context of EV energy consumption computation, electrochemical theory based models require battery-level data like voltage and current while the models using driving parameters such as speed and acceleration generally use basic principles of physics to estimate power consumption. Chan (2000) provides an overview of various electrochemical process based methods. Plett (2004) proposes an extended Kalman-Filtering based method for the battery management system of Lithium-Lead based hybrid EV battery packs. While these methods are essential for battery SOC estimation, it is not practical to use them for the traffic-related perspective here due to their battery data requirements. Battery SOC per unit time can be computed by ADVISOR, a tool developed by the National Renewable Energy Laboratory (NREL) to analyze vehicle performance and fuel economy (Johnson, 2002; Wipke et al., 1999). It uses basic physics and model component performance to replicate the vehicle drivetrain process (NREL, 2013). Maia et al. (2011) use a simulator called Simulation of Urban Mobility (SUMO) to simulate the

energy consumption of EVs. Wu et al. (2015) use test vehicles installed with an in-vehicle data collection system to measure and analyze EV energy consumption. Tanaka et al. (2008) perform a similar study to determine EV power consumption under different speed profiles. Yao et al. (2013) propose a SOC estimation method based on dynamometer test data. Van Haaren (2012) analytically compute energy power consumption for EVs and estimate the parameters through curve-fitting based on the Tesla Roadster data published by Straubel (2008). This study uses the battery model proposed by Van Haaren (2012) due to its computational efficiency and capability to capture battery recuperation.

2.3 Electric vehicle energy-efficient routing

Related to energy-efficient routing, Sachenbacher et al. (2011) introduces the problem of finding the most energy-efficient path for EVs with recuperation in a graph-theoretical context. Artmeier et al. (2010) and Storandt (2012) propose revised shortest-path algorithms to address energy-optimal routing. They formulate energy-efficient routing in the presence of rechargeable batteries as a special case of the constrained shortest path problem and propose adaptations of existing shortest path algorithms. Ichimori et al. (1983) and Adler et al. (2014) address the EV shortest-walk problem to determine the route from an origin to a destination with minimum detouring; this route may include cycles for detouring to recharge batteries. Adler and Mirchandani (2014) further study the online routing and scheduling of EVs that involve wait time as well as a reservation scheme to have a fully-charged battery in place due to limited capacity at a battery swap station. Schneider et al. (2014) investigate the EV routing problem with custom time windows and battery-charging stations in a dynamic context. However, they consider the travel time to be independent of flow in the routing model.

2.4 Electric vehicle traffic assignment models

In the context of EV traffic assignment, Jiang et al. (2012) formulate a multi-class path constrained traffic assignment model for mixed traffic flow with BEVs and ICEVs. In their model, BEV is a vehicle class with trip length no more than the driving range of full

battery capacity, and thus BEVs' equilibrium routes are restricted to the set of distance-constrained paths. However, they do not consider energy recuperation using RBS. Later, Jiang and Xie (2014) extend their model to the combined mode choice and assignment framework by assuming different travel cost functions for BEVs and ICEVs. He et al. (2014) study the network equilibrium of BEVs with recharging capabilities. They propose to minimize the traditional user equilibrium term plus the recharging time. The energy consumption is used to compute the set of usable paths. However, they consider travel time (including recharging time) minimization as the single decision criterion for route choice, and neglect the energy consumption factor in the cost function. In addition, their models focus on static traffic equilibrium rather than dynamic user equilibrium (DUE). Most traffic assignment related studies assume that the electricity consumption is simply a linear function of the distance traveled and the route travel time (He et al., 2014; Jiang and Xie, 2014). However, energy consumption is closely related to travel speed, terrain, battery SOC, temperature, etc. For example, Figure 1 shows the energy consumption rate versus speed for the Tesla Roadster as presented by Van Haaren (2012).

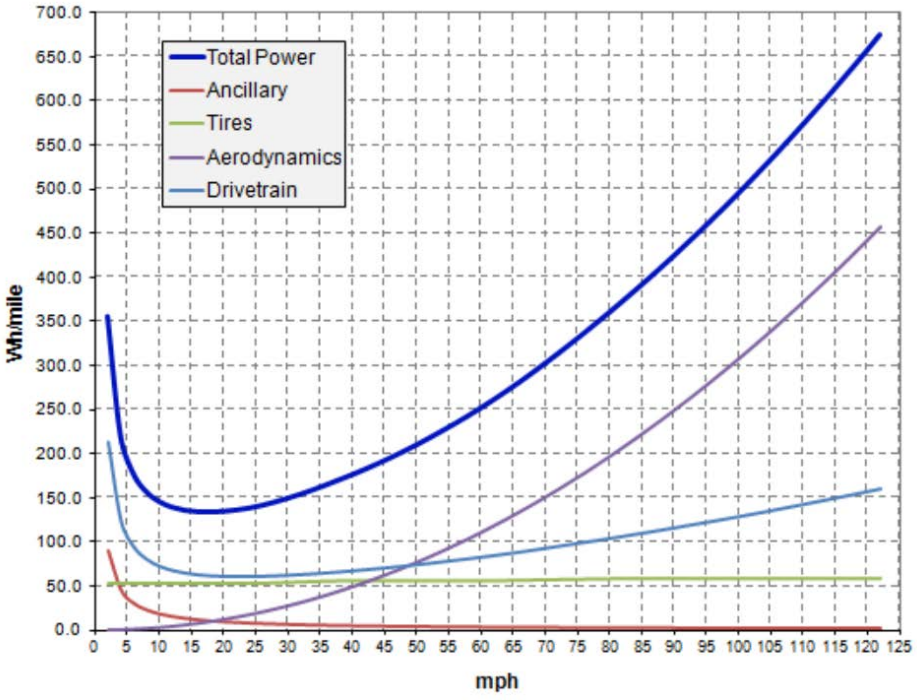

Figure 1 Tesla Roadster Energy Consumption (Van Haaren, 2012)

2.5 Charging station facility location problem

Several studies have investigated the facility location problem of charging stations (Chen et al., 2013; He et al., 2013; Hess et al., 2012; Xi et al., 2013) and battery-swapping stations (Mak et al., 2013) where depleted batteries can be recharged or exchanged en route on long trips. Nie and Ghamami (2013) analyze the selection of battery size and charging capacity to meet a given level of service such that social cost is minimized. He et al. (2013) investigate the charging station location problem for PHEVs. The assumption is that PHEVs are always charged at trip destinations, and that travelers jointly select routes and destinations based upon charging prices at destinations. Note that range limitation is not an issue just for BEVs, but also applies to vehicles with alternative fuels which need to find refueling facilities to successfully complete the trip. Several studies have addressed refueling facility location for alternative fuel based trips (Kuby and Lim, 2005; Upchurch et al., 2009; Wang and Lin, 2009).

2.6 Electric vehicle battery degradation and life estimation models

Two types of battery degradation/aging mechanisms are significant: during storage (calendar aging) and during use (cycle aging). Calendar aging is due to side reactions resulting from thermodynamic instability of active materials, while cycle aging results from kinetic effects, such as structural disordering, or concentration gradients. In past work, the total aging effect is considered as the summation of calendar aging and cycle aging, but interactions may occur (Broussely et al., 2005, 2001; Wright et al., 2002). Battery aging mainly happens at the two electrodes: anode (e.g. graphite) and cathode (e.g. lithium metal oxide). Aging mechanisms occurring at anodes and cathodes are significantly different. Most researchers believe that changes to the Solid Electrolyte Interphase (SEI) due to reactions of the anode with the electrolyte are the major source for aging at the anode (Aurbach et al., 2002; Vetter et al., 2005). Unlike the anode, the cathode can be made using different types of metal oxide materials. Different materials have quite different effects on battery life, and the mechanisms of capacity fade at the cathode are not completely

understood. Moreover, battery aging is induced by various processes and their interactions, and most of them cannot be studied independently (Morrow et al., 2008). Due to the complexity of the Li-ion battery system, some researchers have created semi-empirical battery life models for specific Li-ion battery chemistries based on experimental data (Lee et al., 2015; Purewal et al., 2014; Wang et al., 2014, 2011). Thomas et al. (2008) built a degradation model and an error model using a statistical method based on experimental data.

Using the aforementioned battery life estimation models, some researchers have studied the battery lifespan for EVs/PHEVs (plug-in hybrid electric vehicles). For example, Guenther et al. (2013) studied the EV battery lifespan for different charging behaviors and three speed profiles. Similarly, other studies (Marano et al., 2009) applied speed profiles from standard driving cycles, such as Urban Dynamometer Driving Schedule (UDDS), by either repetition or combination. However, the impacts of realistic vehicle travel patterns with detailed speed profiles on battery lifespans for a large population of EVs have not been studied. As shown in our study results, vehicle travel patterns and driving behavior can have significant impacts on battery lifespan. Using speed profiles from standard driving cycles may be useful under a variety of considerations, but they fail to represent the variation in driving behavior and traffic conditions. Hence, using realistic speed profiles that can capture the effects of traffic conditions will enhance the estimation of EV battery lifespan.

CHAPTER 3. ROUTING ASPECTS OF ELECTRIC VEHICLE DRIVERS AND THEIR EFFECTS ON NETWORK PERFORMANCE

The market share of EVs has increased significantly in recent years (Mock and Yang, 2014) and is likely to increase further in future, due to multiple incentives such as government subsidies, advancement in battery technology and public acceptance of EVs. Shepherd et al. (2012) investigate the effect of multiple factors such as subsidy, average vehicle life and emission rates on the market penetration of BEVs. Becker et al. (2009) predict that EVs, including both PHEVs and BEVs, could comprise 24% of the light-vehicle fleet in USA by 2030. The increase in the market penetration of EVs, especially BEVs, will impact the traffic stream, which may imply new driving and route choice imperatives. BEVs are typically equipped with regenerative braking system (RBS) that can recuperate a part of the kinetic energy lost during the deceleration phase to recharge the battery. This is where braking energy that would otherwise be dissipated as heat is captured and restored in the battery. This can increase the driving range of a BEV. Studies show that in typical urban areas, the recuperation could increase range by about 20%, and often more in hilly areas (Artmeier et al., 2010). Due to the long battery recharging time, en route recharging is usually not an attractive option for BEVs currently, and thus energy-efficient driving and energy recuperation are important factors for BEV drivers. There are two important factors that can encourage a BEV driver to select an energy-efficient route rather than the traditional least travel time route: (i) reduce the operating cost, and (ii) improve the driving range. A BEV driver needs to pay for electricity to charge the battery. In addition, with every charge-discharge cycle, battery life degrades. Therefore, a BEV driver may prefer a route with extra travel time but with reduced energy consumption to decrease operating cost. Because the initial state-of-charge (SOC) of electric battery may not always be full before starting a trip, or the travel distance may be close to the driving range, some BEV drivers may face the dilemma of range anxiety because of the fear of running out of battery charge before completing the trip. In such a situation, a BEV driver may select a

route with higher level of congestion to recuperate a part of kinetic energy lost to recharge the battery so as to improve the range. In addition, for BEVs, energy consumed per unit distance traveled is lower at moderate speed than at higher speed. This can further incentivize BEV drivers to select more congested routes under range anxiety. The presence of BEVs in the traffic stream with the above characteristics of route choice raises two interesting questions: (i) whether the incentives in terms of energy savings and range improvement, and the range anxiety factor, can lead to different route selection by BEV drivers as compared to the ICEV drivers, and (ii) whether this difference in route choice behavior can affect network performance in terms of system travel time. These two questions form the motivation for this study.

This study evaluates the network performance under equilibrium conditions for mixed traffic flow with BEVs and ICEVs by accounting for the difference in their route choice behavior. A multi-class dynamic user equilibrium (MCDUE) model is proposed to investigate the equilibrium of traffic network. The BEVs' route choice behavior is modeled by considering the tradeoff between travel time and energy consumption, and the range anxiety. A microscopic simulation-based solution procedure is proposed to enable accurate computation of energy consumption by using a detailed speed profile rather than a simple function of distance. The effect of battery recuperation is also factored in estimating energy consumption. Thus, the effect of traffic conditions on energy consumption, and subsequently the route choice of BEVs, is captured in a realistic manner. BEV range anxiety is modeled as a step function that triggers when the remaining battery SOC is less than a pre-specified threshold percentage. This introduces nonlinearity in the travel cost function. As part of the solution procedure, a time-dependent least cost path problem for BEVs is developed as a mixed integer linear model by considering a nonlinear travel cost function.

The study experiments show that ICEVs prefer to choose routes with least travel time while BEVs desire routes with slower speeds to save energy and/or improve range. Based on the current and near future prospects of technology, BEVs will have maximum fuel-efficiency at lower speeds (~15mph) while ICEVs are fuel-efficient in moderate speed

range (~45mph). Due to the need for energy-efficiency and range improvement in the route selection for BEVs, the network performance in terms of average travel time and average battery SOC consumption (energy consumption as a percentage of battery capacity) is also analyzed.

This study has contributions for both theory and practice. In a theoretical context, it provides an analytical treatment where the congestion and energy imperatives of ICEVs and BEVs, respectively, are synergistically traded off. This potentially has the synergistic implication that the traffic system performance can be enhanced beyond that of a traffic stream with only ICEVs. This study also extends the current literature related to BEV routing by incorporating the effect of range anxiety in route choice behavior realistically by considering accurate battery SOC consumption based on detailed speed profile rather than a simple function of distance. From a practical perspective, this result provides insights to decision-makers on analyzing BEV route choice to manage network-wide traffic conditions towards system optimum without exclusively using just monetary instruments like tolling or congestion pricing, at least under mixed traffic environments.

3.1 Multi-Class Dynamic User Equilibrium Model (MCDUE)

3.1.1 Problem statement

We consider a mixed traffic scenario consisting of BEV and ICEV drivers whose route choices are based on the DUE principle with respect to the generalized cost. That is, they seek the individual least time-dependent generalized cost in their route selection. The generalized cost for BEVs includes three components: (1) route travel time, (2) energy consumption, and (3) cost reflecting range anxiety when the remaining SOC level is below a certain threshold. The generalized cost for ICEVs includes only the route travel time. Different from the more extensively studied analytical single user class DUE (Peeta and Ziliaskopoulos, 2001), the problem is modeled as a multiple user class DUE formulation with two vehicle classes (BEVs and ICEVs). This study extends the single user class DUE formulation proposed by Ban et al. (2008) as a complementarity problem to multiple user classes.

3.1.2 MCDUE formulation

The notations used are as follows:

Sets:	
G	Network, $G \equiv (N, A)$;
N	Set of nodes;
A	Set of links;
T	Time horizon;
R	Set of origins;
S	Set of destinations;
$\mathcal{M}$	Set of vehicle classes, $\mathcal{M} \equiv (E, I)$;
E	BEV class;
I	ICEV class;
$A(i)$	Set of outbound links of node $i \in N$;
$B(i)$	Set of inbound links of node $i \in N$;
K_{rs}	Set of simple paths from origin $r \in R$ to destination $s \in S$;
L_k	Sequence of links in path $k \in K_{rs}$.
Indices:	
t	Time period, $t \in T$;
t_d	Departure time period, $t_d \in T$;
i	Node, $i \in N$;
a	Link, $a \in A$;
r	Origin node, $r \in R$;
s	Destination node, $s \in S$;
m	Vehicle class, $m \in \mathcal{M}$;
h_a	Head node of link a;
l_a	Tail node of link a;
k	Path, $k \in K_{rs}$.
Parameters:	
$d_{is}^m(t)$	Time-dependent travel demand from node $i \in N$ to destination $s \in S$ for each vehicle class m in time period $t \in T$
ϑ	Value of time;
α	Coefficient of energy cost for BEV class;
γ	Coefficient of range anxiety cost for BEV class;
ω	Range anxiety threshold percentage;
$\mathcal{K}$	Battery capacity.

Variables:

$\tau_a(t)$	Travel time on link a in time period t;
$\mathcal{S}_a(t)$	Energy consumed on link a in time period t;
$C_a^m(t)$	Generalized travel cost for vehicle class m on link a in time period t;
$\pi_{is}^m(t)$	Minimum generalized travel cost from node i to destination s for vehicle class m in time period t;
$\tau_a(t)$	Travel time on link a in time period t;
$u_{as}^m(t)$	Inflow rate into link a bound for destination s for vehicle class m in time period t;
$v_{as}^m(t)$	Exit flow rate from link a bound for destination s for vehicle class m in time period t;
$x_{as}^m(t)$	Flow on link a bound for destination s for vehicle class m in time period t;
$u_a^m(t)$	Inflow rate into link a for vehicle class m in time period t;
$v_a^m(t)$	Exit flow rate from link a for vehicle class m in time period t;
$f_{rs,k}^E(t_d)$	Flow on path k from origin r to destination s departing in time period t_d for BEV class;
$\mathcal{S}_T$	Total energy consumption;
β	Variable associated with range anxiety cost; 0 if the total energy consumption ($\mathcal{S}_T$) is less than or equal to range anxiety threshold $\omega * \mathcal{K}$, γ otherwise.

Under DUE, the generalized travel costs of all utilized time-dependent routes for the same departure time are equal and less than or equal to those of unutilized routes. For the MCDUE, this principle holds for each vehicle class. The MCDUE can be formulated as a complementarity problem using Equation (1). The mathematical operator $p \perp q$ denotes that p is perpendicular to q, that is, $p^T q = 0$. Equation (1) implies that for each vehicle class $m \in \mathcal{M}$, the inflow rate $u_{as}^m(t)$ into link a bound for destination s in time period t can be non-zero only if the generalized travel cost $C_a^m(t)$ on link a in time period t is equal to the difference between the minimum generalized travel cost $\pi_{l_a s}^m(t)$ from tail node l_a of link a to destination s in time period t and the minimum generalized travel cost $\pi_{h_a s}^m\big(t + \tau_a(t)\big)$ from head node h_a of link a to destination s in time period $t + \tau_a(t)$, where $\tau_a(t)$ is the travel time on link a in time period t.

$$0 \le u_{as}^{m}(t) \perp \left\{C_a^m(t) + \pi_{h_a s}^{m}\left(t + \tau_a(t)\right) - \pi_{l_a s}^{m}(t)\right\} \ge 0 \qquad \forall m, a, s, t \tag{1}$$

Generalized cost functions

As discussed earlier, the generalized travel cost functions are different for the two vehicle classes. For ICEVs, the generalized cost includes travel time only; for BEVs it includes travel time, energy related costs and range anxiety if the remaining battery SOC level is below a threshold. The BEV and ICEV drivers select the least cost routes based on the generalized travel cost. The energy related costs account for both monetary (electricity consumption cost) and non-monetary (such as long-recharging time, battery degradation, etc.) costs related to energy consumption. To incorporate range anxiety behavior, when the remaining SOC is less than a pre-specified threshold percentage (ω) of the battery capacity ($\mathcal{K}$), a cost associated with range anxiety ($\beta = \gamma$) is imposed for the BEV. Otherwise, it is assumed that there is no range anxiety issue for the BEV driver, that is, the range anxiety cost is zero ($\beta = 0$). Also, while the range anxiety threshold can vary across drivers, we assume it to be homogeneous across BEV drivers in both the study formulation and experiments to focus on understanding the network effects of range anxiety by using the notion of low anxiety and high anxiety drivers. Further, the heterogeneity in range anxiety threshold can be seamlessly incorporated by extending the study formulation through the use of multiple BEV classes in the proposed MCDUE.

The generalized travel cost functions for BEVs ($C_a^E(t)$) and ICEVs ($C_a^I(t)$) on link a in time period t are defined using Equations (2) and (3). These cost functions involve two variables, $\tau_a(t)$ and $\mathcal{S}_a(t)$, representing travel time and energy consumption on link a in time period t respectively. The parameters ϑ, α and γ refer to value of time, coefficient of energy related costs and cost associated with range anxiety, respectively.

$$C_a^E(t) = \vartheta \cdot \tau_a(t) + \alpha \cdot \mathcal{S}_a(t) + \beta \cdot \mathcal{S}_a(t) \qquad \forall a, t \tag{2}$$

$$C_a^I(t) = \vartheta \cdot \tau_a(t) \qquad \forall a, t \tag{3}$$

$$\beta = \begin{Bmatrix} \gamma & if\ S_T \geq \omega * \mathcal{K} \\ 0 & otherwise \end{Bmatrix}$$

Mass balance constraints

The mass balance constraints ensure that the flow for each vehicle class m bound for destination s is conserved for every link $a \in A$ in each time period $t \in T$, that is, the rate of change of link flow $x_{as}^{m}(t)$ is the difference between inflow rate $u_{as}^{m}(t)$ and exit flow rate $v_{as}^{m}(t)$. This constraint is expressed in Equation (4).

$$\frac{dx_{as}^{m}(t)}{dt} = u_{as}^{m}(t) - v_{as}^{m}(t) \qquad \forall m, a, s, t \qquad (4)$$

Flow conservation constraints

These constraints ensure that the flow for each vehicle class m bound for destination s is conserved at every node $i \in N$ in each time period $t \in T$; the total outbound flow from a node is equal to the demand originating at that node ($d_{is}^{m}(t)$) plus the total inbound flow at that node. This constraint is expressed as:

$$\sum_{a \in A(i)} u_{as}^{m}(t) = d_{is}^{m}(t) + \sum_{a \in B(i)} v_{as}^{m}(t) \qquad \forall m, i, s, t \qquad (5)$$

FIFO constraints

The first-in first-out (FIFO) principle states that vehicles departing later cannot, on average, exit a link earlier; that is, vehicles must exit the link later than the vehicles that entered earlier than them. While FIFO may not always hold in reality as vehicles can overtake others, for aggregated flow this constraint is satisfied. FIFO constraints can be represented as:

$$t_1 + \tau_a(t_1) \leq t_2 + \tau_a(t_2) \qquad \forall\ t_1 < t_2 \qquad (6)$$

Flow propagation constraints

The flow propagation constraints describe the spatial and temporal traffic flow dynamics at the macroscopic level (Astarita, 1996) as shown in Equation (7). In particular,

these constraints depict the relationship between combined inflow rate in time period t and combined exit flow in time period $t + \tau_a(t)$ of all vehicle classes with change in travel time $\tau_a(t)$ of link a in time period t. These constraints are synergistic with the FIFO principle. They are based on the assumption that driving characteristics, such as maximum speed and acceleration, of all vehicle classes are similar.

$$\sum_{m \in \mathcal{M}} v_{as}^{m}\big(t + \tau_a(t)\big) = \frac{\sum_{m \in \mathcal{M}} u_{as}^{m}(t)}{1 + {d\tau_a(t)}/{dt}} \qquad \forall a, s, t \qquad (7)$$

Definitional constraints

Equation (8) expresses the aggregated inflow rate $u_a^m(t)$ and exit flow rate $v_a^m(t)$ over all destinations for link a and vehicle class m in time period t. Equation (9) illustrates the aggregated link flow $x_a^m(t)$ over all destinations for link a and vehicle class m in time period t. Equations (10) and (11) are the non-negativity constraints for flow and cost variables.

$$u_a^m(t) = \sum_{s \in S} u_{as}^m(t), \qquad v_a^m(t) = \sum_{s \in S} v_{as}^m(t) \qquad \forall m, a, t \qquad (8)$$

$$x_a^m(t) = \sum_{s \in S} x_{as}^m(t) \qquad \forall m, a, t \qquad (9)$$

$$u_{as}^m(t) \geq 0, \qquad v_{as}^m(t) \geq 0, \qquad x_{as}^m(t) \geq 0, \qquad \forall m, a, s, t \qquad (10)$$

$$\pi_{l_{as}}^m(t) \geq 0, \qquad \pi_{h_{as}}^m(t) \geq 0, \qquad \forall m, a, s, t \qquad (11)$$

Feasibility constraints

Feasibility constraints are required to address two issues associated with BEVs: (i) that the trip length does not exceed the BEV battery capacity; (ii) the need to circumvent the possibility of cycles that may arise due to negative link costs for BEVs. We assume that BEV recharging occurs at either origin or destination, and there is no en route charging. Let $f_{rs,k}^E(t_d)$ be the BEV flow on a simple path $k \in K_{rs}$ from origin r to destination s in

departure time period t_d. Equation (12) illustrates that the inflow rate $u_{as}^{E}(t)$ of BEVs on link a bound for destination s in time period t is the sum of flows from all origins $r \in R$ bound for destination s departing in any time period $t_d \in T$ such that these flows reach link a in time period t. Equation (13) defines an indicator variable $I_{a,t}^{k}(t_d)$ with value equal to 1 if link a is in the sequence of links L_k for path k and the flow departing from origin r to destination s in time period t_d enters link a in time period t, and 0 otherwise. Equations (14) and (15) define a function $\phi_{L_k[j]}(t_d)$ to represent the time period in which the flow departing in time period t_d reaches the j^{th} link in the sequence of links L_k for path k. Note that as variable $\tau_a(t)$ is strictly positive, Equation (15) eliminates the possibility of any cycle in the path. Equation (16) restricts the set of paths K_{rs} to contain paths with minimum generalized cost for every O-D pair rs for every departure time period $t_d \in T$ for BEVs. Equation (17) satisfies the battery capacity constraint for BEVs, that is, the total battery consumption for BEVs on path k from origin r to destination s departing in time period t_d cannot exceed the maximum battery capacity $\mathcal{K}$.

$$u_{as}^{E}(t) = \sum_{\substack{t_d \in T, \\ t_d \le t}} \sum_{r \in R} \sum_{k \in K_{rs}} f_{rs,k}^{E}(t_d) I_{a,t}^{k}(t_d) \qquad \forall a, s, t \tag{12}$$

$$I_{a,t}^{k}(t_d) = \begin{cases} 1 & if\ L_k[j] = a, \phi_{L_k[j]}(t_d) = t \\ 0 & otherwise \end{cases} \qquad \forall j \in I^{+}, j \le |L_k| \tag{13}$$

$$\phi_{L_k[1]}(t_d) = t_d \tag{14}$$

$$\phi_{L_k[j+1]}(t_d) = \phi_{L_k[j]}(t_d) + \tau_{L_k[j]}\left(\phi_{L_k[j]}(t_d)\right) \tag{15}$$

$$\sum_{j=1}^{|L_k|} C_j^{E}\left(\phi_{L_k[j]}(t_d)\right) = \pi_{rs}^{E}(t_d) \qquad \forall r, s, k, t_d \tag{16}$$

$$\sum_{j=1}^{|L_k|} S_a\left(\phi_{L_k[j]}(t_d)\right) \le \mathcal{K} \qquad \forall r, s, k \tag{17}$$

Equations (1) – (17) constitute the complementarity based MCDUE model. The next section presents a solution procedure for it.

3.2 Solution procedure

This section illustrates the solution procedure and summarizes its various components. Analytical methods have been proposed in the literature to solve the complementarity problem (Ban et al., 2008). The complexity of the MCDUE model is similar to that of the DUE formulation proposed by Ban et al. (2008), and hence a similar solution strategy can be used to solve it analytically.

As discussed earlier, the generalized travel cost function of BEVs consists of travel time, energy consumption, and range anxiety if the SOC level is below a threshold. The energy consumed and its regeneration due to RBS depend on the microscopic speed profile, particularly the speed and acceleration profiles. These microscopic details of speed profiles, and hence the percentage of battery charge consumed and its regeneration, are difficult to express in an analytical closed form, precluding the use of an analytical solution approach. Therefore, an iterative solution procedure is adopted to solve the MCDUE model. The solution procedure uses a microscopic traffic simulator, an energy consumption model, a time-dependent least cost path algorithm, and a path-flow update mechanism in each iteration.

3.2.1 Solution procedure

Figure 2 illustrates the steps of the solution procedure. The solution procedure is initialized using a fixed time-dependent origin-destination (O-D) demand for each vehicle class. In the 0th iteration, a set of path flows is determined using all-or-nothing (AON) assignment for each O-D pair for each vehicle class for all time periods. Then, a microscopic traffic simulator (using AIMSUN (Barceló and Casas, 2005; Casas et al., 2010)) is used for network loading to obtain vehicle travel times and BEV speed profiles based on the initial set of path flows. The energy consumption for BEVs is computed using Haaren's model (Van Haaren, 2012) based on BEVs speed profiles (see Section 3.2.3). The

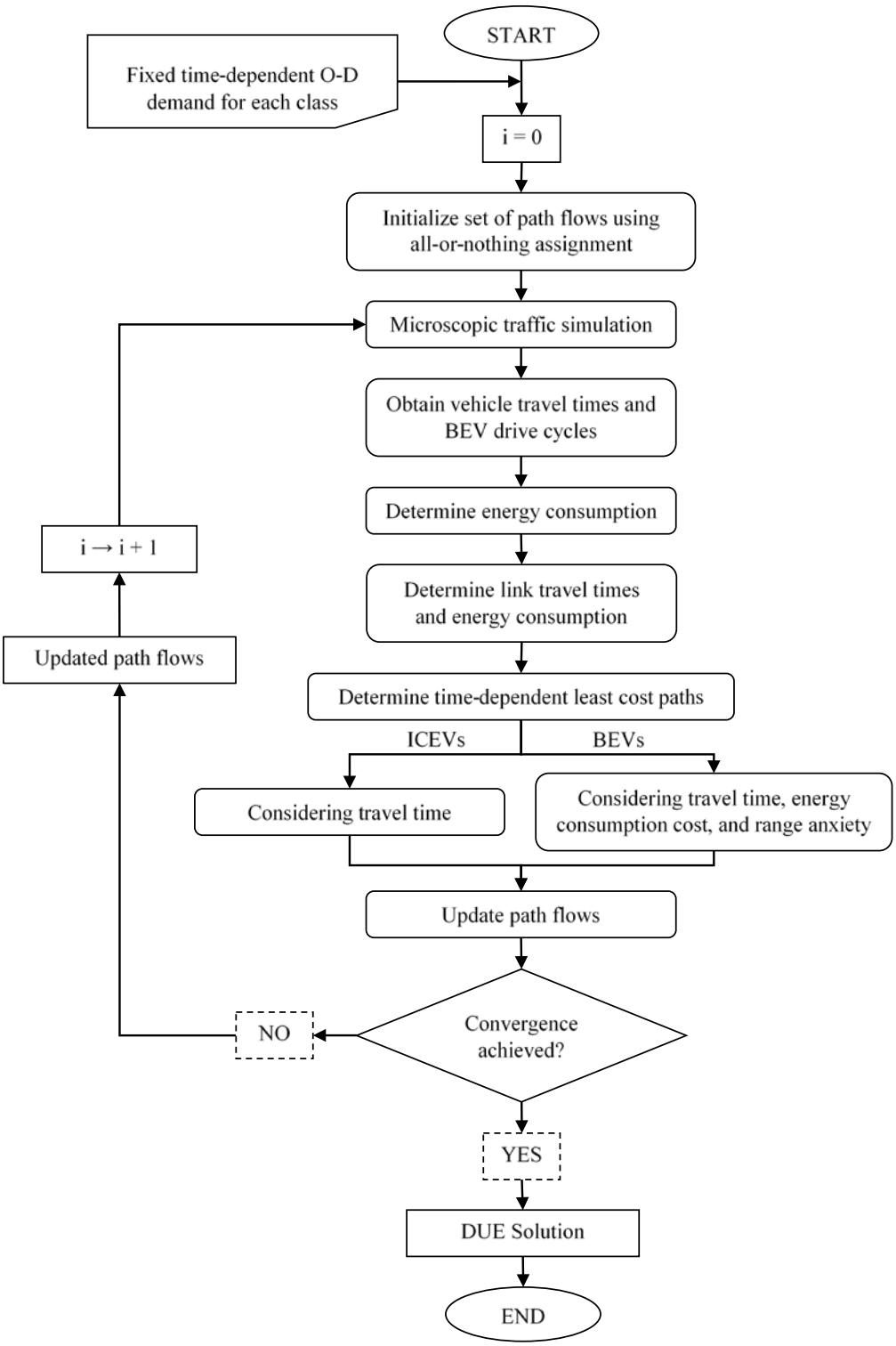

Figure 2 Solution Procedure

energy consumption and travel time for each link in each time period are determined by taking the average of energy consumed and travel time experienced on that link, respectively, for all vehicles entering the link in corresponding time period. Next, the time-dependent least (generalized) cost paths (TDLCPs) are determined for both ICEVs and BEVs. For ICEVs, the time, energy related costs and range anxiety. The computed TDLCPs are appended to their corresponding path set if they are already not in that set. The path flows for each O-D pair for each vehicle class for all time periods are updated simultaneously using a modified version of a flow update mechanism proposed by Smith (Smith, 1984). The iteration counter is updated by 1. The updated path flows are simulated using AIMSUN to generate the vehicle travel times and BEV speed profiles. This process is continued until convergence is achieved, which occurs when the average of the difference between the generalized path travel cost of each path of each O-D pair and the lowest generalized path travel cost for that O-D pair is less than 5% of the lowest generalized path travel cost.

3.2.2 Role of microscopic simulation

The generalized link travel cost for a BEV includes the battery SOC which requires the vehicle's speed profile as input to compute energy consumption. Microscopic traffic simulation software AIMSUN is used to obtain link travel times and BEV speed profiles. In zeroth iteration, the simulation is performed using path flows based on AON assignment. In future iterations, the generated TDLCPs and the corresponding flows obtained using the modified Smith's mechanism for both vehicle classes for each O-D pair for all time periods are provided as input to AIMSUN. Hence, the role of microscopic traffic simulation in this study is to generate BEV speed profiles and vehicle travel times.

3.2.3 Electric vehicle energy consumption model

The model proposed by (Van Haaren, 2012) is used to compute battery energy consumption. It considers power losses at constant speed (V) and variable speed separately. The power loss at constant speed (P_{cons}) is the sum of the losses due to aerodynamics (P_{aer}), drive-train (P_{dr}), rolling resistance (P_{rr}) and ancillary losses (P_{anc})

as shown in Equations (18) to (22). The energy loss at constant speed (E_{cons}) is the summation of power loss over time for the time duration of a vehicle's speed profile ($\mathcal{D}$). A moving vehicle has two types of kinetic energy (E_{kin}): linear (E_{lin}) and rotational (E_{rot}). Energy loss at variable speed is due to change in kinetic energy (ΔE_{kin}). For computational simplicity, the model assumes that the rotational kinetic energy is about 5% of linear kinetic energy. During acceleration phase, the electric energy is converted into kinetic energy with about 85% efficiency (β_{eff}). During deceleration phase, a part of lost kinetic energy is recuperated as electric energy with efficiency (β_{rbs}) of around 40%. The rate of change of kinetic energy (ΔE_{kin}) and the energy conversion from battery-to-wheel and vice versa Thus, the total energy consumption is the net sum of energy losses at constant speed (E_{cons}), energy loss during acceleration phase (E_{acc}) and energy recuperation during deceleration phase (E_{dec}). As stated earlier, the model parameters are based on empirical data from Tesla Roadster, as shown in Table 1. The quality of the model results depends on the time resolution of the speed profile data (δ); the study experiments use 1-second speed profile data.

$$P_{aer} = \frac{1}{2}\rho A C_d V^3 \tag{18}$$

$$P_{dr} = \alpha_{dr} V^3 + \beta_{dr} V^2 + \gamma_{dr} V + c_{dr} \tag{19}$$

$$P_{rr} = c_{rr} m g V \tag{20}$$

$$P_{anc} = 1.0 \tag{21}$$

$$P_{cons} = P_{aer} + P_{dr} + P_{rr} + P_{anc} \tag{22}$$

$$E_{cons} = \sum_{k=1}^{\mathcal{D}/\delta} P_{cons}^{k} * \delta \tag{23}$$

$$E_{kin} = E_{lin} + E_{rot} \approx 1.05 * E_{lin} \tag{24}$$

$$E_{lin} = \frac{1}{2} m V^2 \tag{25}$$

$$E_{acc} = \frac{\Delta E_{kin}}{\beta_{eff}} \quad (26)$$

$$E_{dec} = \beta_{rbs} * \Delta KE \quad (27)$$

Table 1 Parameters of the energy consumption model (Van Haaren, 2012)

Parameter	Definition	Value
C_d	Drag coefficient	0.29
ρ	Air density (kg/m3)	1.2
A	Vehicle front area (m2)	2.27
α_{dr}	Drivetrain coefficient 1	4*10-6
β_{dr}	Drivetrain coefficient 2	5*10-4
γ_{dr}	Drivetrain coefficient 3	0.0293
c_{dr}	Drivetrain coefficient 4	0.375
c_{rr}	Rolling resistance coefficient	0.0075
m	Vehicle mass (kg)	1520
g	Gravity (m/s2)	9.81
β_{eff}	Battery to motor efficiency	0.85
β_{rbs}	Regeneration efficiency	0.4

3.2.4 Time-Dependent Least Cost Path (TDLCP) algorithm

As illustrated in Figure 1, in each iteration the TDLCP algorithm identifies a TDLCP for each vehicle class in each time period for each O-D pair. This path is appended to the corresponding path set if it is not already in it. Flows are shifted from paths with higher generalized costs to those with lower generalized costs (see Section 3.2.5 for the flow update process).

TDLCPs for BEVs

For BEVs, the generalized cost consists of travel time, energy related costs and the cost associated with range anxiety. The travel time and SOC on each link in each time period are obtained from AIMSUN. To solve the TDLCP problem, we construct a time-expanded network $G^t(N^t, A^t)$ from the original network $G(N, A)$ as follows. For each time period t, a copy of nodes N is created. For each link $a \in A$, if its travel time in time period t is $\tau_a(t)$, a link $b \in A^t$ in time-expanded network connecting from node l_a in time period t to node h_a in time period $t + \tau_a(t)$ is constructed. Thus, the travel time of the newly constructed

link (τ_b) is equal to $\tau_a(t)$, and the energy consumed on the newly constructed link ($\mathcal{S}_b$) is equal to $\mathcal{S}_a(t)$. The TDLCP for BEVs is to find the least generalized cost path in G^t by solving the following mathematical formulation.

The notations used are as follows:

Sets:	
G^t	Time-expanded network;
N^t	Set of nodes in G^t;
A^t	Set of links in G^t;
r^t	Origin node in G^t;
s^t	Destination node in G^t;
Indices:	
b	Link, $b \in A^t$;
Parameters:	
τ_b	Travel time on link $b \in A^t$;
$\mathcal{S}_b$	Energy consumed on link $b \in A^t$;
M	Sufficiently large positive number;
Variables:	
f_{ij}	Decision variable, $f_{ij} \in \{0,1\}$, $f_{ij} = 1$ if link $(i,j) \in A^t$ is selected, 0 otherwise;
y	Auxiliary variable, $y \in \{0,1\}$.

The objective function (28) minimizes the generalized cost that includes three terms: path travel time, energy related costs, and cost associated with range anxiety. Equation (29) is the flow conservation constraint, implying that one unit of flow is sent from source r^t to sink s^t in G^t. Constraint (30) specifies that the energy consumed along the path is bounded by the BEV's battery capacity $\mathcal{K}$, that is, a BEV cannot run out of battery charge en route. Equations (31) – (34) state that if $\sum_{b \in A^t} \mathcal{S}_b \cdot f_b \geq \omega \cdot \mathcal{K}$, then $y = 1$ and $\beta = \gamma$, otherwise $y = 0$ and $\beta = 0$. This implies that the cost associated with range anxiety is triggered only if the battery SOC consumed is more than the specific threshold percentage of battery (ω). If the SOC is below the threshold percentage of battery charge, there is no range anxiety issue for the BEV driver and $\beta = 0$. The parameter M, also known

as “big M”, allows a binary variable to switch a constraint on or off. In this model, the minimum value of M should be at least $\mathcal{K}$.

$$\min\left(\vartheta \cdot \sum_{b\in A^t} \tau_b \cdot f_b + \alpha \sum_{b\in A^t} \mathcal{S}_b \cdot f_b + \sum_{b\in A^t} \beta \cdot \mathcal{S}_b \cdot f_b\right) \tag{28}$$

$$\sum_{(i,j)\in A^t} f_{ij} - \sum_{(j,i)\in A^t} f_{ji} = \begin{cases} 1 & if\ i = r^t \\ -1 & if\ i = s^t \\ 0 & otherwise \end{cases} \qquad \forall i \in N^t \tag{29}$$

$$\sum_{b\in A^t} \mathcal{S}_b \cdot f_b \le \mathcal{K} \tag{30}$$

$$-M(1-y) \le \sum_{b\in A^t} \mathcal{S}_b \cdot f_b - \omega \cdot \mathcal{K} \le M(y) \tag{31}$$

$$-M(1-y) \le \beta - \gamma \le M(1-y) \tag{32}$$

$$-My \le \beta \le My \tag{33}$$

$$y \in \{0,1\}, f_b \in \{0,1\} \qquad \forall b \in A^t \tag{34}$$

Equations (28) – (34) specify a constrained shortest path problem as a mixed integer formulation. Note that the third term of objective function is nonlinear, which makes the model difficult to solve. Hence, next, we linearize the nonlinear term.

Introduce a dummy variable μ_b such that $\mu_b = \beta \cdot f_b$. Then, the objective function be expressed as Equation (35). The constraint set (36) – (39) indicates that if $f_b = 1,\ \mu_b = \beta$; otherwise $f_b = 0$, then $\mu_b = 0$. Then, the objective function (35) is linear. In summary, Equations (29) – (39) represent a mixed integer linear program (MILP) that is solved to obtain the TDLCPs for the BEV class. The proposed MILP is solved using IBM ILOG CPLEX 12.5 MILP solver (CPLEX, 2012).

$$\min\left(\vartheta \cdot \sum_{b\in A^t} \tau_b \cdot f_b + \alpha \cdot \sum_{b\in A^t} \mathcal{S}_b \cdot f_b + \sum_{b\in A^t} \mu_b \cdot \mathcal{S}_b\right) \tag{35}$$

$$\mu_b \leq \beta \qquad \forall b \in A^t \qquad (36)$$

$$\mu_b \geq \beta - M(1 - f_b) \qquad \forall b \in A^t \qquad (37)$$

$$\mu_b \geq 0 \qquad \forall b \in A^t \qquad (38)$$

$$\mu_b \leq M \cdot f_b \qquad \forall b \in A^t \qquad (39)$$

TDLCPs for ICEVs

For ICEVs, the generalized travel cost consists of travel time only. The travel time on each link in each time period is obtained from AIMSUN. Then, the decreasing order of time (DOT) algorithm (Chabini, 1998) is implemented to compute the time-dependent shortest paths. These paths are used to update the path set for ICEVs in each time period for each O-D pair.

3.2.5 Path flow update process

After the TDLCPs are computed in an iteration, they are appended to their corresponding path set and path costs are updated for all paths in the set. The path sets for both vehicle classes for all O-D pairs for each time period are updated simultaneously using the modified Smith's mechanism (Smith, 1984).

Modified Smith's mechanism

The notations are used as follows:

Sets:	
W	Set of origin-destination (O-D) pairs;
P_{wt}^m	Set of paths for vehicle class m and O-D pair w in time period t
Indices:	
w	O-D pair, $w \in W$;
i, j	Indices for paths, $i, j \in P_{wt}^m$;
Variables:	
$C_{wt}^m(i)$	Generalized travel cost for vehicle class m and O-D pair w on path i in time period t;
$\Delta C_{wt}^m(i,j)$	Generalized travel cost difference between path i and path j for vehicle

	class m and O-D pair w in time period t;
$\Delta\hat{C}_{wt}^{m}(i,j)$	Normalized cost difference between path i and path j for vehicle class m and O-D pair w in time period t;
f_{wt}^{m}(i)	Flow on path i for vehicle class m and O-D pair w in time period t;
Δf_{wt}^{m}(i)	Change in flow on path i for vehicle class m and O-D pair w in time period t;
f^{*m}_{wt}(i)	Updated flow on path i for vehicle class m and O-D pair w in time period t;

Step 1: For each time period and each O-D pair, compute the difference in generalized cost between each path pair for each vehicle class:

$$\Delta C_{wt}^{m}(i,j) = C_{wt}^{m}(i) - C_{wt}^{m}(j) \qquad \forall m,w,t,i,j \qquad (40)$$

Step 2: Normalize the generalized cost difference using the difference between the maximum and the minimum generalized cost for a vehicle class for each O-D pair and each time period:

$$\Delta\hat{C}_{wt}^{m}(i,j) = \frac{\Delta C_{wt}^{m}(i,j)}{\max\limits_{k\in P_{wt}^{m}}(C_{wt}^{m}(k)) - \min\limits_{k\in P_{wt}^{m}}(C_{wt}^{m}(k))} \qquad \forall m,w,t,i,j \qquad (41)$$

Step 3: Obtain the move direction by summing the inflows and outflows for each path as follows:

$$\Delta f_{wt}^{m}(\mathrm{i}) = \sum_{j,\Delta\hat{C}_{wt}^{m}(i,j)\geq 0} \Delta\hat{C}_{wt}^{m}(i,j) * f_{wt}^{m}(\mathrm{i}) + \sum_{j,\Delta\hat{C}_{wt}^{m}(i,j)<0} \Delta\hat{C}_{wt}^{m}(i,j) * f_{wt}^{m}(\mathrm{j}) \qquad \forall m,w,t,i \qquad (42)$$

Step 4: Simultaneously update the path flows for both vehicle class for all O-D pairs for all time periods using step size α. The step size α is the inverse of the iteration number. Then, the equation for path flow update is as follows:

$$f^{*m}_{wt}(i) = f_{wt}^{m}(i) + \alpha * \Delta f_{wt}^{m}(i) \qquad \forall m,w,t,i \qquad (43)$$

The flow update mechanism presented heretofore is obtained through three important modifications to Smith's flow update mechanism. First, it uses multiple vehicle classes and the temporal dimension to reflect flow propagation of BEVs and ICEVs along various links, unlike the static context of Smith's mechanism where a path flow is considered to be present on all links of that path simultaneously. Second, it normalizes the cost difference (see Equation (41)) before determining the move direction of the flow update process, leading to improved convergence. Third, it updates the path flow vectors for both vehicle classes for all time periods for all O-D pairs simultaneously to eliminate order bias in the flow update process.

3.3 Numerical experiments

3.3.1 Experiment setup

Figure 3 illustrates the network used for the study experiments. It consists of 35 nodes, 68 links, 7 origins/destinations and 42 O-D pairs with non-zero demand. Origins and destinations are marked through A - G. The network has four types of links: freeway, two-lane arterial, one-lane arterial, and ramps. The arterials are connected to the freeway through 12 ramps at three interchanges.

The experiments are conducted for a one-hour horizon of interest preceded by a 15-minute warm-up period. Hence, the time horizon is divided into 75 time periods of 1 minute each. The simulation is allowed to run until all vehicles exit the network beyond the 75-minute horizon. The base O-D demand for the time horizon is presented in Table 2. The demand for each time period is computed by multiplying the base O-D demand with the temporal demand distribution factors shown in Figure 4. The demand for the warm-up period is identical to that of the first time period, and the demand for the clearance period is zero. The demand for each vehicle class is determined by its market penetration.

The value of travel time for both ICEVs and BEVs is assumed to be $20 per hour. In the numerical experiments, the energy related costs are captured by factoring the non-monetary cost component through an increase in the coefficient value for the electricity consumption cost. The cost of electricity and the BEV range anxiety threshold are varied

to perform sensitivity analysis. The effect of the BEV market penetration on network performance is also analyzed.

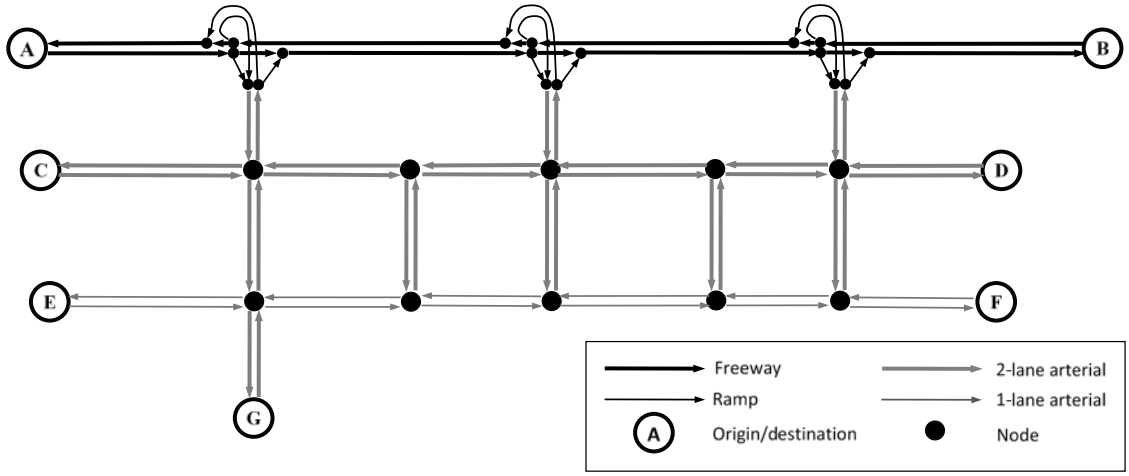

Figure 3 Study Network

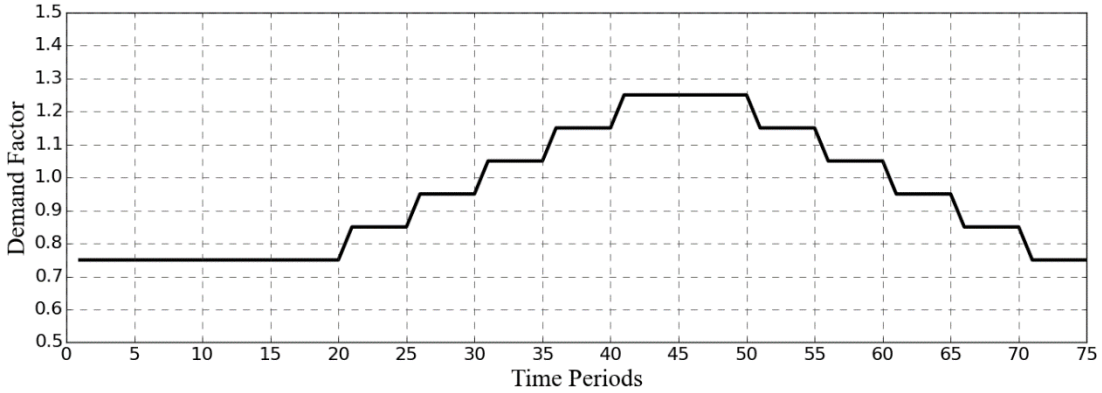

Figure 4 Temporal Distribution of Demand Factors

Table 2 Base Demand for the Time Horizon

O/D	A	B	C	D	E	F	G
A	0	3000	160	250	70	70	100
B	3000	0	375	100	125	50	300
C	75	100	0	100	40	35	75
D	75	50	100	0	50	25	100
E	75	100	40	50	0	50	40
F	75	40	40	25	40	0	40
G	125	150	75	100	100	50	0

3.3.2 Effect of BEV market penetration

Sensitivity analysis is performed for BEV market penetration under the scenario with no range anxiety. The electricity cost is assumed to be 50 cents/kWh as the fee to recharge a BEV at a commercial level 2 charging station may range between 30 cents/kWh to 80 cents/kWh (Blink, 2015). Figure 5 illustrates the effect of the BEV market penetration on the travel time distribution of BEVs and ICEVs. The average travel time of ICEVs is less than that of BEVs, implying that BEVs trade off their travel time for savings in energy consumption while ICEVs prefer routes with least travel time. Further, the system performance in terms of the total system travel time (TSTT) improves as the market penetration of BEVs increases. This is because as the BEV market penetration increases, more BEVs shift from freeway to arterials, thereby enhancing the performance of freeway as illustrated by Figure 6. Since freeway flows are typically larger than arterial flows, this shift tends to have a positive impact on overall network performance with the BEV market penetration increase. Hence, the preference of some BEVs to choose paths with higher travel time to save battery SOC consumption or recuperate battery charge moves the network towards system optimality in terms of TSTT. Though the total number of vehicles on freeway decreases with increase in BEV market penetration, the number of BEVs on freeway increases leading to the general trend of reduction in BEV average travel time.

While it is expected that an increase in market penetration of BEVs should increase the average travel time of BEVs, the opposite trend is observed in Figure 5. This phenomenon can be explained as follows. As the total travel demand is fixed, an increase in market penetration implies that more BEVs from all O-D pairs shift to arterial routes except for the O-D pairs A-B and B-A (refer Figure 3) for which the freeway still remains the optimal route. Therefore, with an increase in market penetration of BEVs, the overall traffic volume on the freeway decreases. Thus, the average travel time of ICEVs decreases as most of them use the freeway route and its travel time decreases due to the decrease in volume. The average travel times of BEVs for O-D pairs A-B and B-A also decreases as most of them use the freeway route. Since, the travel demand for these two O-D pairs is significantly larger than for the other O-D pairs (refer Table 2), the weighted decrease in

travel time of BEVs of these O-D pairs outweighs the weighted increase in travel times of all other O-D pairs. Therefore, an overall decrease in system level average travel time is observed.

The effect of market penetration on the average BEV battery SOC consumption is illustrated in Figure 7. The average battery SOC consumption increases with the increase in market penetration of BEVs because the number of ICEVs decreases, and hence more number of BEVs are present on freeway (see Figure 6). Due to the relatively higher speed on freeway compared to arterials coupled with the fact that higher speed increases energy consumption (see Section 3.2.3), the average battery SOC consumption increases as the number of BEVs on freeway increases with market penetration.

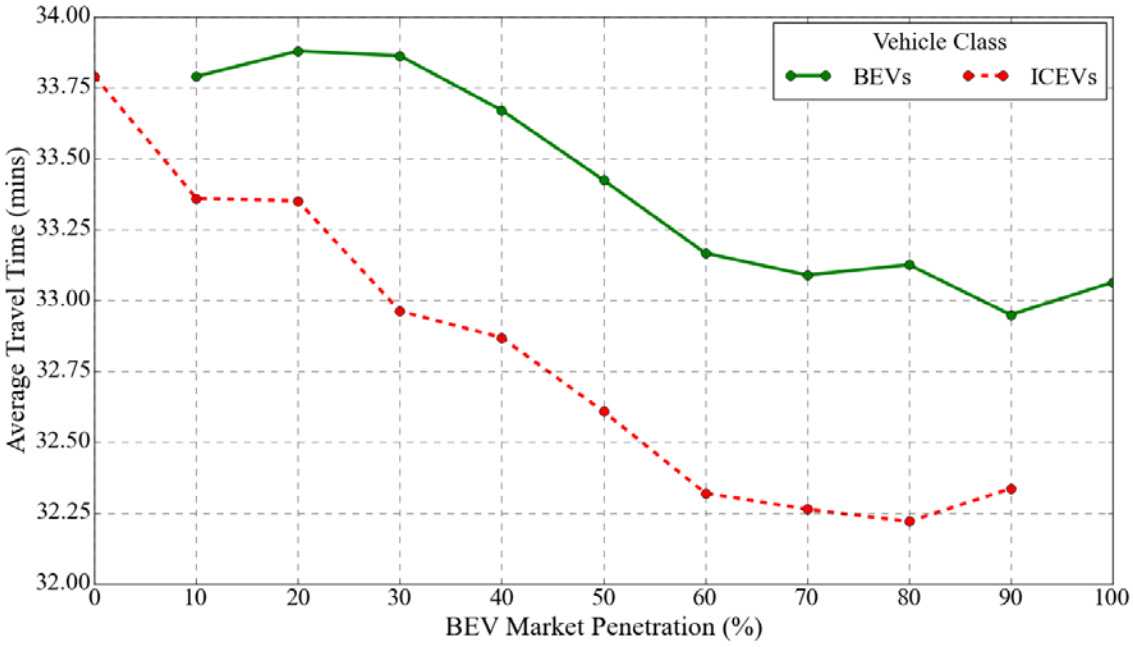

Figure 5 Effect of BEV Market Penetration on Average Travel Time

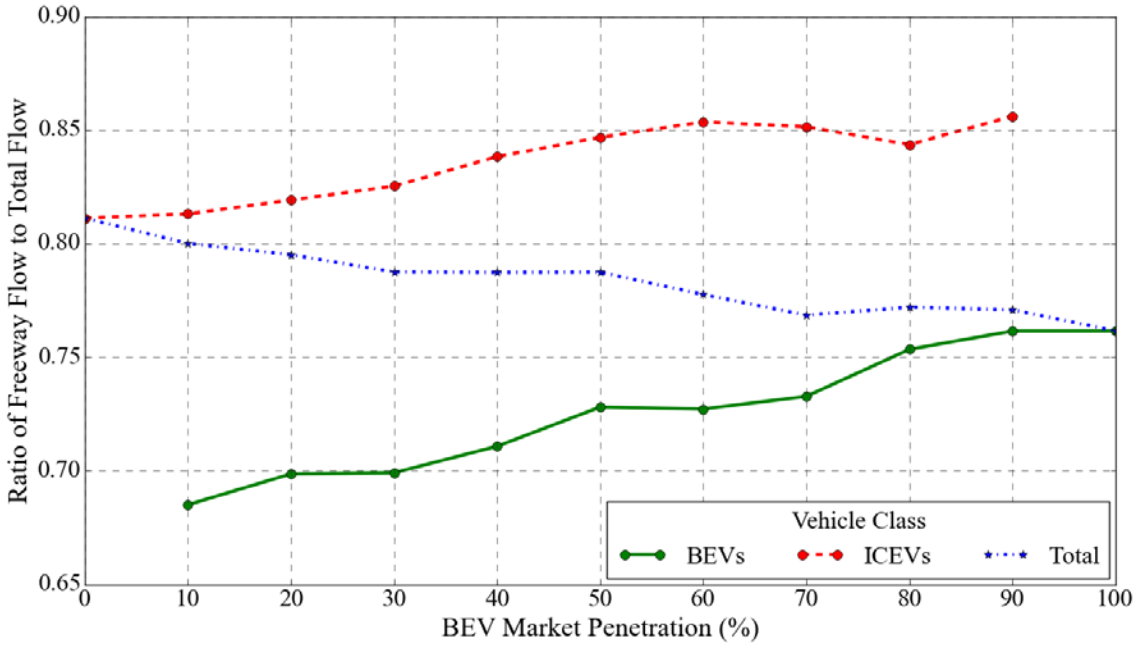

Figure 6 Effect of BEV Market Penetration on Freeway Flows

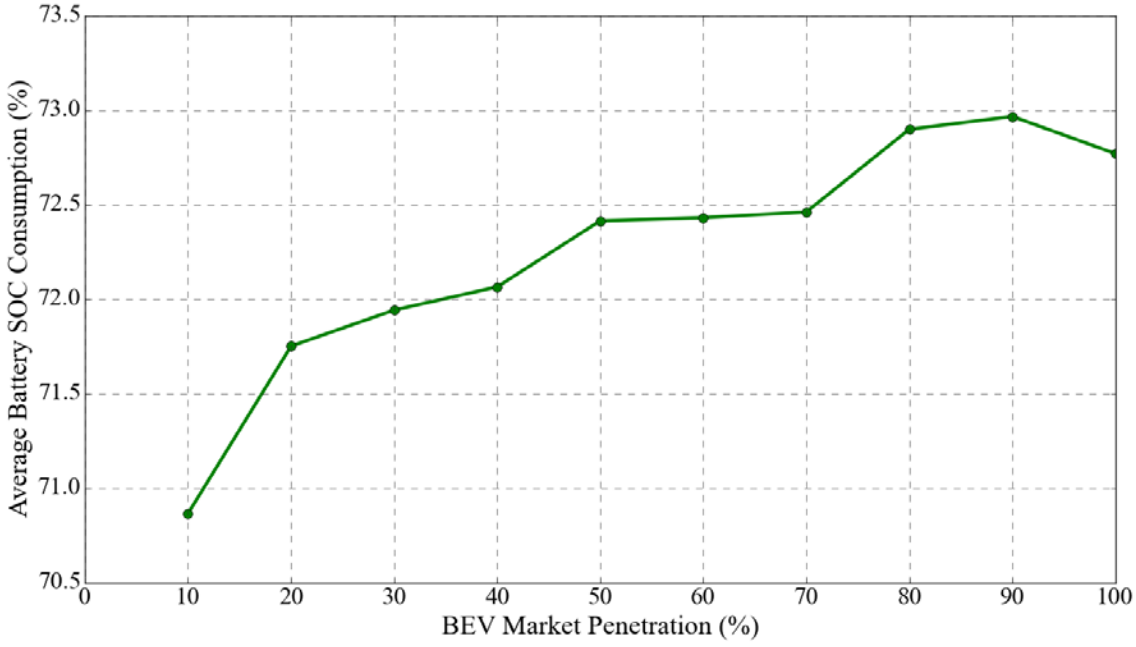

Figure 7 Effect of BEV Market Penetration on Battery SOC Consumption

3.3.3 Effect of electricity cost

The effect of electricity cost on network performance is analyzed for the case with no range anxiety and equal market penetration of BEVs and ICEVs. Figure 8 shows the relationship between average travel time and electricity cost. The average travel time reduces for ICEVs with an increase in electricity cost, but has an overall negative effect on BEVs. At low electricity costs, the magnitude of positive effect for ICEVs is slightly higher than that for BEVs leading to an overall positive effect for the system. Akin to the discussion in Section 3.3.2, the increase in average travel time for BEVs and decrease for ICEVs can be explained by the shift in the flow of BEVs from freeway to arterials, as illustrated in Figure 9. At higher electricity costs, more BEVs shift from freeway to arterials as they have more incentive to save on energy consumption though these routes are longer in terms of travel time. This initially leads to a decrease in freeway travel time, thereby causing a decrease in average travel time for both BEVs and ICEVs. At the higher range of electricity costs, a large fraction of BEVs shift to arterials leading to high congestion. While this large shift by BEVs leads to further decrease in average travel time for ICEVs on freeway, the increase in travel time of BEVs on arterials more than negates benefits on freeway and causes system level increases in average travel time. As a result, average travel time of the system increases beyond a certain electricity cost.

The effect of electricity cost on the average battery SOC consumption for BEVs is illustrated in Figure 10, which indicates that the average battery SOC consumption decreases with electricity cost increase. As the electricity cost increases, BEVs have more incentive to shift to routes with lesser battery SOC consumption, and hence more BEVs shift from freeway to arterials (as shown in Figure 9). Due to the relatively lower speed on arterials compared to freeway, the battery SOC consumption decreases (see Section 3.2.3).

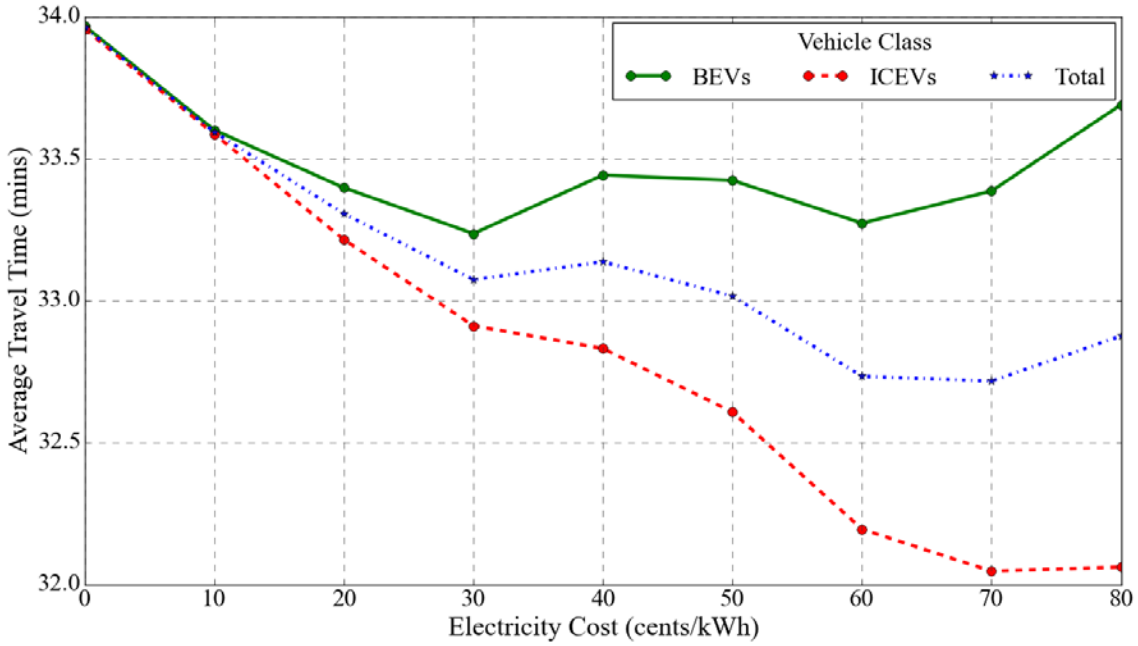

Figure 8 Effect of Electricity Cost on Average Travel Time

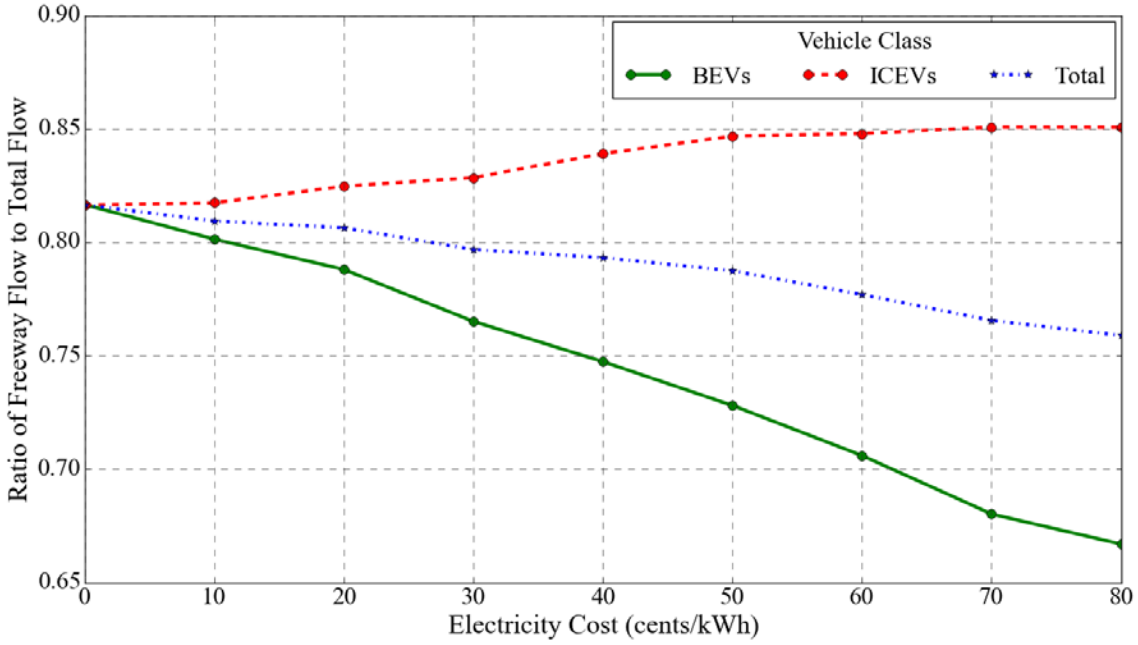

Figure 9 Effect of Electricity Cost on Freeway Flow

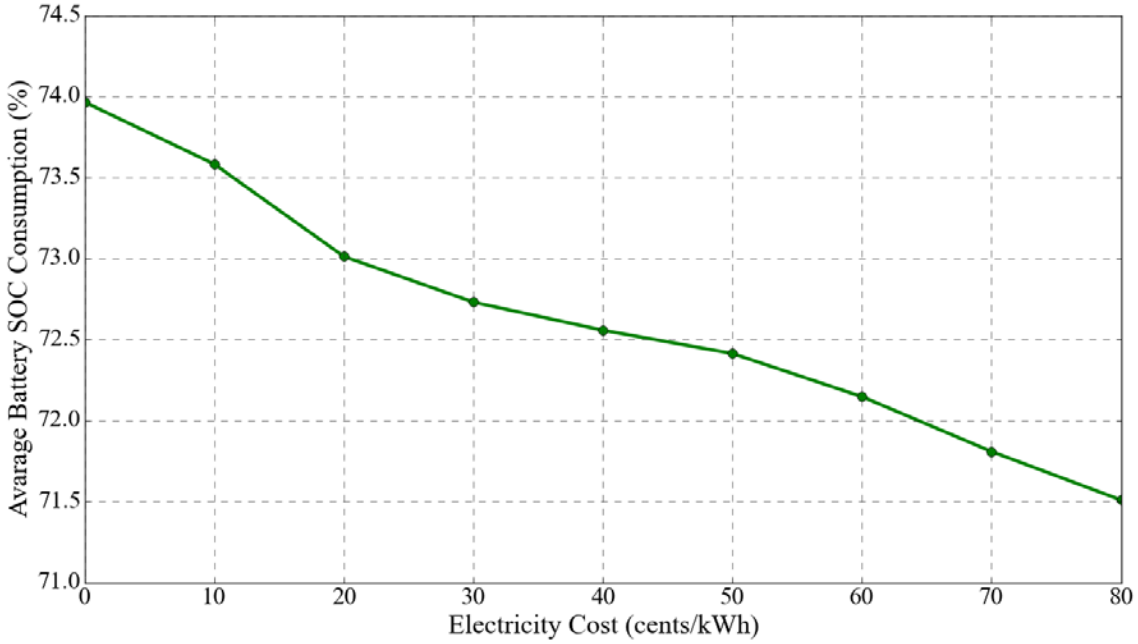

Figure 10 Effect of Electricity Cost on Battery SOC Consumption

3.3.4 Effect of range anxiety

To analyze the effect of range anxiety, it is classified into low range anxiety and high range anxiety. A driver with high range anxiety is more reluctant towards consuming battery SOC and feels anxious at a relatively higher level of remaining battery capacity compared to a driver with low range anxiety. The typical percentage of battery SOC consumption on the freeway route in the study network is around 75-80%. Hence, high range anxiety is assumed to be triggered when a BEV consumes 70% of the battery capacity (that is, 30% battery is remaining) and low range anxiety is assumed to be triggered when 90% of the battery capacity (that is, 10% battery is remaining) is consumed. Figure 11 illustrates the effect of range anxiety on travel time distribution of BEVs and ICEVs for an electricity cost of 50 cents/kWh and equal market penetration of ICEVs and BEVs. It indicates that high range anxiety has a negative impact on the network performance as BEVs experience higher travel times under high range anxiety compared to the case of low range anxiety. Vehicles with travel time of around 20 minutes in the network are typically

those for which destinations are relatively closer to their origins and mostly use arterial routes (see Figure 3). At high range anxiety, a significant number of BEVs use routes with higher travel time to reduce battery SOC consumption and hence shift from freeway to arterial routes. This causes severe congestion on the arterial routes and has a negative impact on the travel time of the vehicles on arterial routes, including vehicles whose trips partly involve arterial travel. Hence, all vehicles including ICEVs experience relatively higher travel times under high range anxiety, with BEVs performing slightly worse than ICEVs, on average.

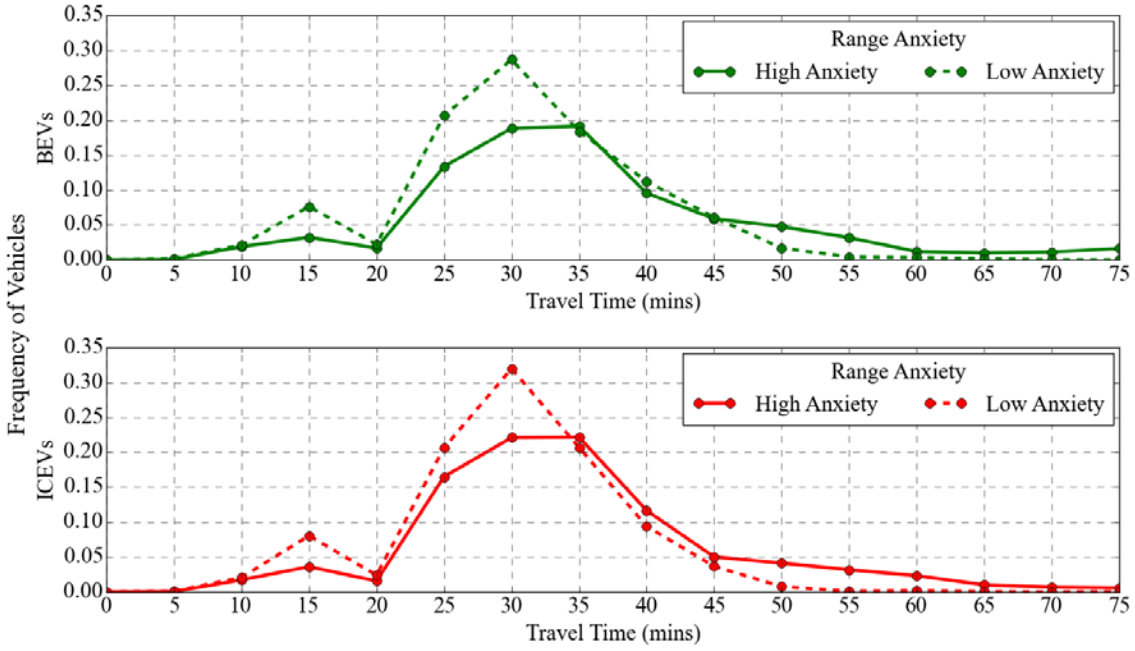

Figure 11 Effect of Range Anxiety on Travel Time Distribution

3.3.5 Effect of congestion level

The effect of congestion level on route selection by BEVs is analyzed for the case of equal market penetration, an electricity cost of 50 cents/kWh and without range anxiety. Congestion levels are classified as free flow, mild congestion, moderate congestion and high congestion based on average network speeds of about 50 mph, 31 mph, 21 mph and 15 mph, respectively. Figure 12 shows the ratio of freeway flow to total flow for BEVs and ICEVs. The freeway flow for both ICEVs and BEVs decreases with increase in congestion

and the difference between freeway flow of ICEVs and BEVs decreases as well. With increase in congestion, the travel time on freeway route increases, and hence vehicles tend to move to alternative routes. Under free flow, BEVs save on electricity cost by selecting arterial routes as they have slower speeds. As congestion increases, the average speeds on both freeway and arterials decrease, reducing the incentive for BEVs to select arterial routes. Hence, as congestion increases, BEV behavior is closer to that of ICEVs in terms of route selection.

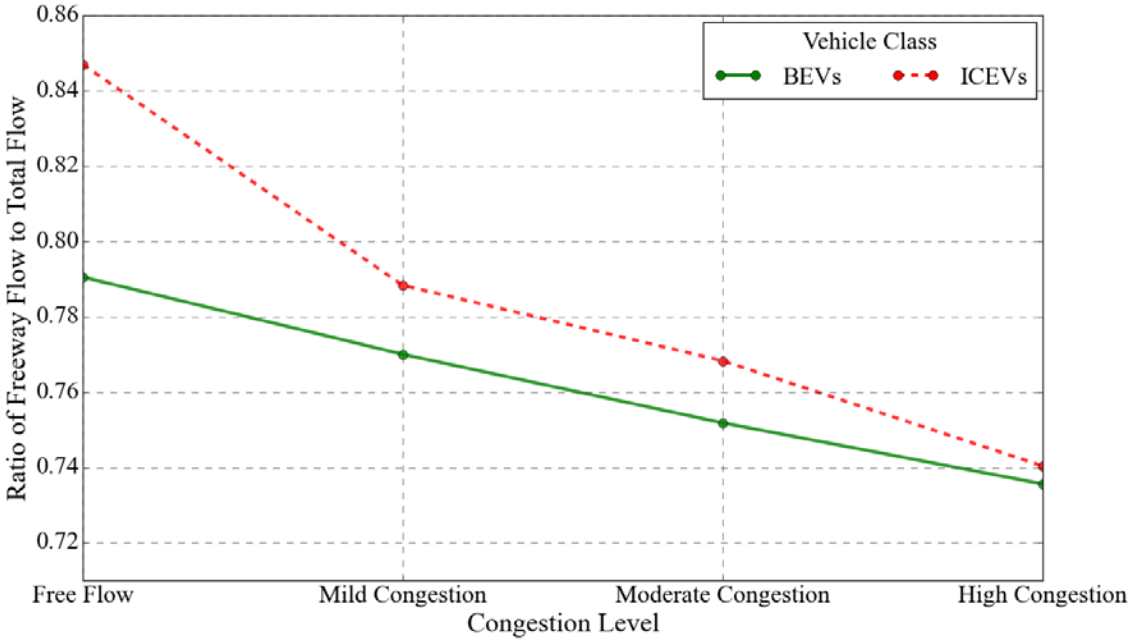

Figure 12 Effect of Congestion Level on Freeway Flow

Figure 13 shows the effect of traffic congestion on average battery SOC consumption. The average battery SOC consumption decreases up to the moderate congestion level and then increases slightly for the high traffic congestion level. This can be explained using the relationship between speed and energy consumption per mile for BEVs in Figure 1. The energy-efficiency for BEVs is lowest under free flow as the vehicles consistently drive at high speeds. As congestion increases, the speed decreases, and up to a certain point the average battery SOC consumption also decreases. Under high congestion, though the average network speed is about 15 mph, a good proportion of BEVs

travel at very low speeds (less than 10mph) for a major portion of their trip with low energy-efficiency, increasing their average battery SOC consumption.

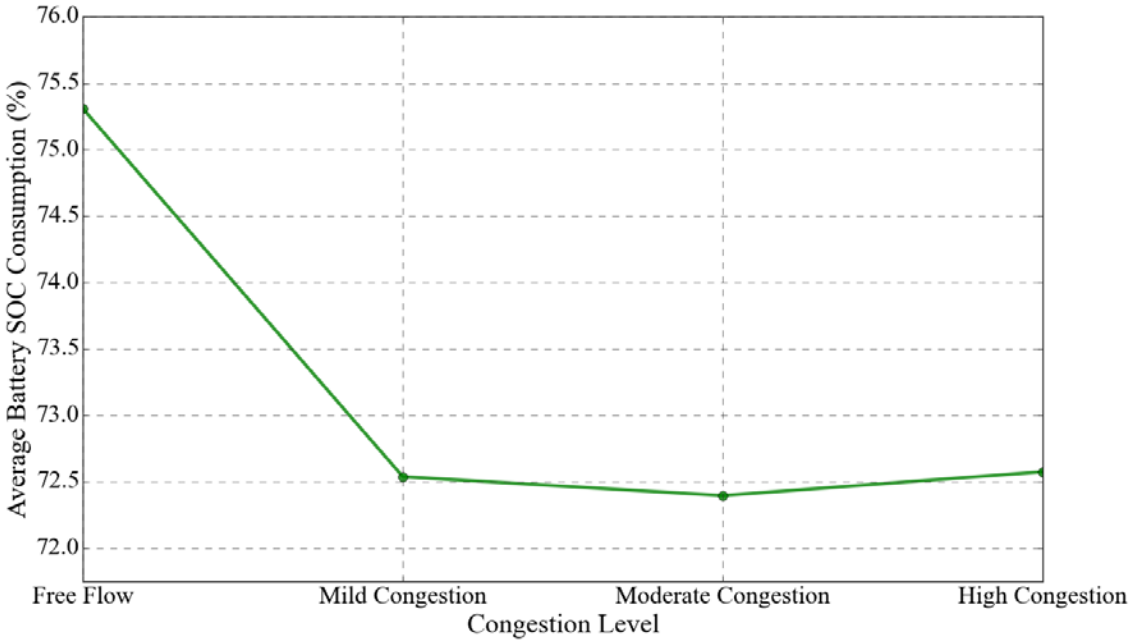

Figure 13 Effect of Congestion Level on Battery SOC Consumption

3.3.6 Insights from numerical experiments

The numerical experiments illustrate that, based on the generalized travel cost, BEV drivers in general tend to shift from the route with lower travel time (freeways) to routes with higher travel times (arterials) to reduce electricity costs and avoid range anxiety. This route choice aspect of some BEVs reduces freeway congestion and benefits other vehicles using the freeway, but consequently increases congestion on arterial routes. The overall network performance is the net effect of these contrasting phenomena. In a network such as the one considered for the study experiments, where freeway flow is significantly higher than that of arterials, BEVs will have a positive impact on the overall network performance.

The route choice behavior tends to have a positive impact on overall system performance under both an increase in BEV market penetration and electricity cost. However, under very high BEV market penetration or at very high electricity cost, increased congestion on arterials more than negates the freeway benefits, leading to

reduced system performance. The average battery SOC consumption of BEVs increases with their market penetration as more BEVs are on freeway, while it decreases with increase in electricity cost as they have more incentive to shift to arterial routes.

As traffic congestion increases, average network speed decreases, thereby reducing incentive for BEVs to select alternative routes to save on energy consumption. This increases the relative importance of travel time in the BEV route choice behavior, reducing the difference in route choice behavior of BEVs and ICEVs. The average battery SOC consumption decreases with increase in congestion until the moderate traffic congestion level. Under the high congestion level, the average battery SOC consumption increases as the vehicles travel a major portion of their trip at very low speeds (less than 10 mph) which is not energy-efficient for BEVs.

In summary, BEV route choice imperatives can synergistically lead to improved network performance under mixed traffic conditions for traffic networks with high levels of freeway flow and the availability route alternatives involving arterials.

CHAPTER 4. QUANTIFYING THE IMPACTS OF ELECTRIC VEHICLE TRAVEL PATTERNS ON BATTERY LIFESPAN

The majority of EVs in the market use a Li-ion battery pack with an energy capacity of around 20 kWh. For example, the battery pack energy capacity for the Nissan leaf is 24 kWh, Honda Fit EV is 20 kWh, Ford Focus Electric is 23 kWh, and Smart EV is 17.6 kWh. The energy capacity of a battery pack degrades with time and usage (Broussely et al., 2005; Guenther et al., 2013; Purewal et al., 2014; Vetter et al., 2005; Wang et al., 2014, 2011). As the energy capacity decreases, the vehicle range drops. An oft-stated common criterion is that the battery should be retired from the vehicle application if its capacity has depleted to 70-80% of its original capacity (Broussely et al., 2005; Saxena et al., 2015; Vetter et al., 2005). The replacement of a battery pack poses significant cost to vehicle owners, though batteries can be resold and utilized for other applications such as renewable energy storage (Huang et al., 2012; Neubauer and Pesaran, 2011; Wood et al., 2011). Under this common battery replacement criteria, well-designed battery warranty strategies will play a crucial role in widespread EV adoption. However, among the current commercialized EVs available in the market, only Nissan Leaf has a battery capacity warranty against degradation from regular use. Under this warranty, Nissan will repair or replace a Leaf's battery within five years or 60,000 miles if it loses more than 30 percent of its energy capacity (DeMuro, 2013). Therefore, quantifying EV battery lifespan for a large population of EVs is important for vehicle manufacturers, car owners, and battery researchers seeking to support practical applications.

This study quantifies EV battery lifespan for a large population of EVs through a semi-empirical battery aging model and a microscopic traffic simulation model. Realistic speed profiles are generated using microscopic traffic simulation model for the Indianapolis road transportation network. Five different temperature scenarios are examined. The results illustrate the impacts of temperature, total distance traveled, average speed and speed deviation on battery lifespan. This will provide insights for policymakers,

vehicle manufacturers and researchers to improve battery technology, and design regional strategies to promote EV adoption.

4.1 Methodology

A multi-paradigm modeling approach provides the flexibility to study the lifespan characteristics of a population of EVs. It enables different systems to be simulated with the most suitable modeling methods. Population behavior for a transportation network is addressed using building blocks, each of which represents a relevant set of phenomena. By building up theses blocks together, the whole system can be simulated and investigated in a holistic manner. This paper considers four different building blocks: a microscopic traffic network simulation model which provides realistic speed profiles of vehicles, an EV energy consumption model which provides power demand results for different speed profiles, a battery circuit model which converts power demands to current flows, and a semi-empirical battery degradation model which simulates battery lifespan based on current flows and temperature.

Using the microscopic traffic network simulation model, vehicle trips from the National Household Travel Survey (NHTS) of 2009 data are matched with simulated speed profiles that reflect traffic conditions. The speed profile data is then fed into the EV energy consumption model to compute power profiles. The power profiles are used as inputs to the battery circuit model to obtain battery current data. In the end, the battery current data is fed into the battery aging model to simulate EV battery life. Figure 14 shows a simplified flowchart of the methodology framework.

4.1.1 Household vehicle travel patterns

For EVs, travel distance, travel speed, and vehicle acceleration and deceleration all impact battery lifespan. In this study, real-world household vehicle travel information is extracted from the NHTS data. The NHTS data provides daily trip profiles of 150,147 random households across the United States (Federal Highway Administration, 2010). Among the 150,147 households, 4,350 are from the state of Indiana. This study extracts all of the 2,832 samples which are from Indianapolis urban and suburban areas to represent

Indianapolis households. Considering the range of EVs, only samples with daily travel distance less than or equal to 80 miles are selected, resulting in 2,306 (about 81% of 2,832) representative samples of household vehicles. The data includes car type, trip start and end time, trip distance, trip origin and destination, etc.; however, there is no information related to vehicles' speed profiles. In order to get speed profiles, a microscopic traffic network simulation model is built for the city of Indianapolis. This model is used to generate realistic microscopic speed profiles with 1-sec time resolution. The speed profiles are then matched with each vehicle trip from the NHTS data based on trip characteristics to obtain the household vehicle travel patterns.

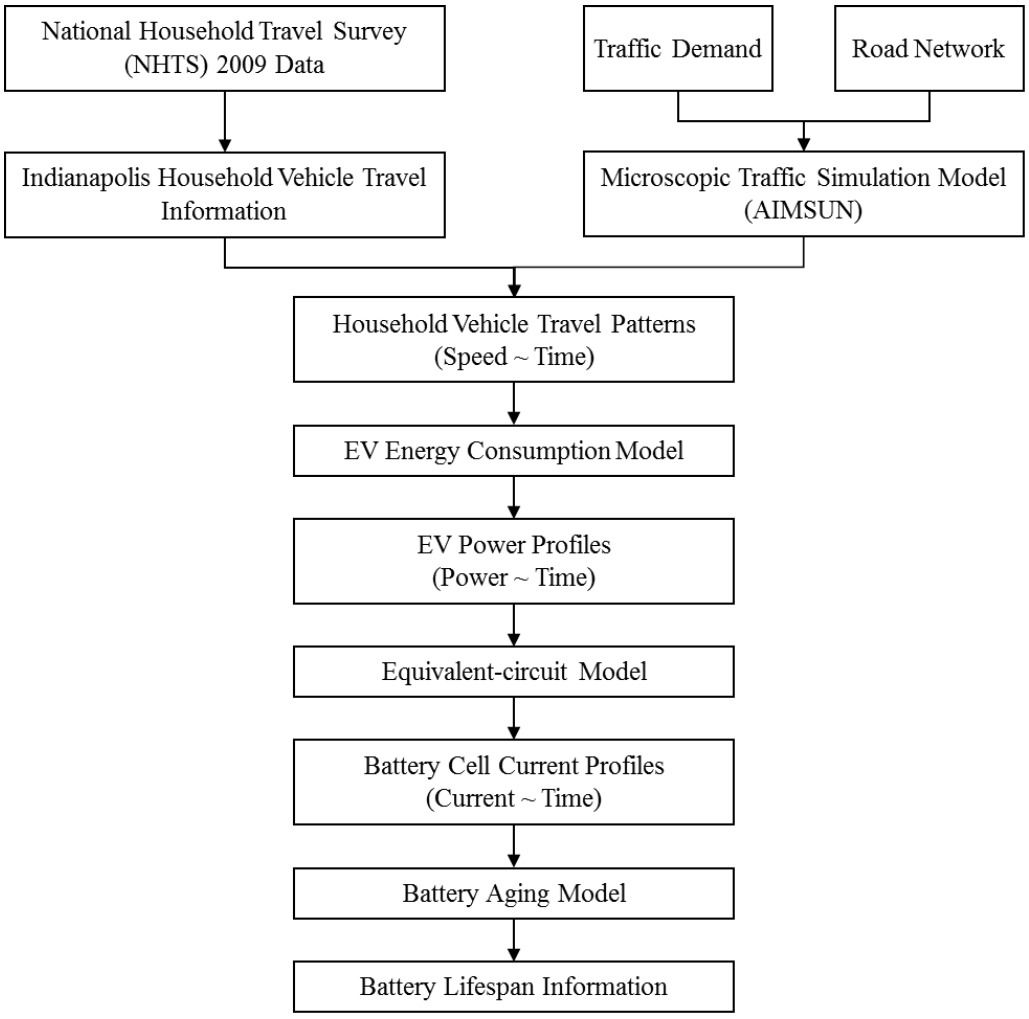

Figure 14 Conceptual flowchart

Traffic simulation techniques are commonly used to capture the interactions between vehicles as well as between vehicles and infrastructure at a microscopic level. A microscopic simulation model employs various models such as car-following, lane-changing, route choice, etc. to mimic real-world conditions. In this study, detailed speed profiles of vehicles are required to compute the battery lifespan of EVs. The traffic network simulation software AIMSUN is used to generate realistic drive-cycles of the vehicles at the microscopic level (Barceló and Casas, 2005; Casas et al., 2010). A detailed road network of Indianapolis is built in AIMSUN. The network contains all the freeways, most of the urban roads and some minor roads as shown in Figure 15. The traffic is simulated for a 24-hour period with discrete 15-minute interval origin-destination (O-D) demand matrices. The traffic demand level is calibrated based on the NHTS data for the state of Indiana.

Figure 15 Indianapolis road network

In AIMSUN, vehicles are assigned to specific routes based on distance and road-type. The trip data for each vehicle from the 2306 samples is obtained by matching to a specific trip in the network based on the trip departure time, trip distance, trip purpose, and freeway route indicator. The trip departure time and trip distance are the primary parameters used for matching. From these, the trip end time will be determined automatically as the speed profile is generated by the network. The trip purpose is used to assign route towards the downtown area or the sub-urban area, and the freeway route indicator is used to check whether the trip uses the freeway. The drive-cycle data from AIMSUN is gathered for specific vehicles that match the trip profiles from NHTS data based on the above criteria. The first plot in Figure 16 shows an example of the vehicle speed profile information.

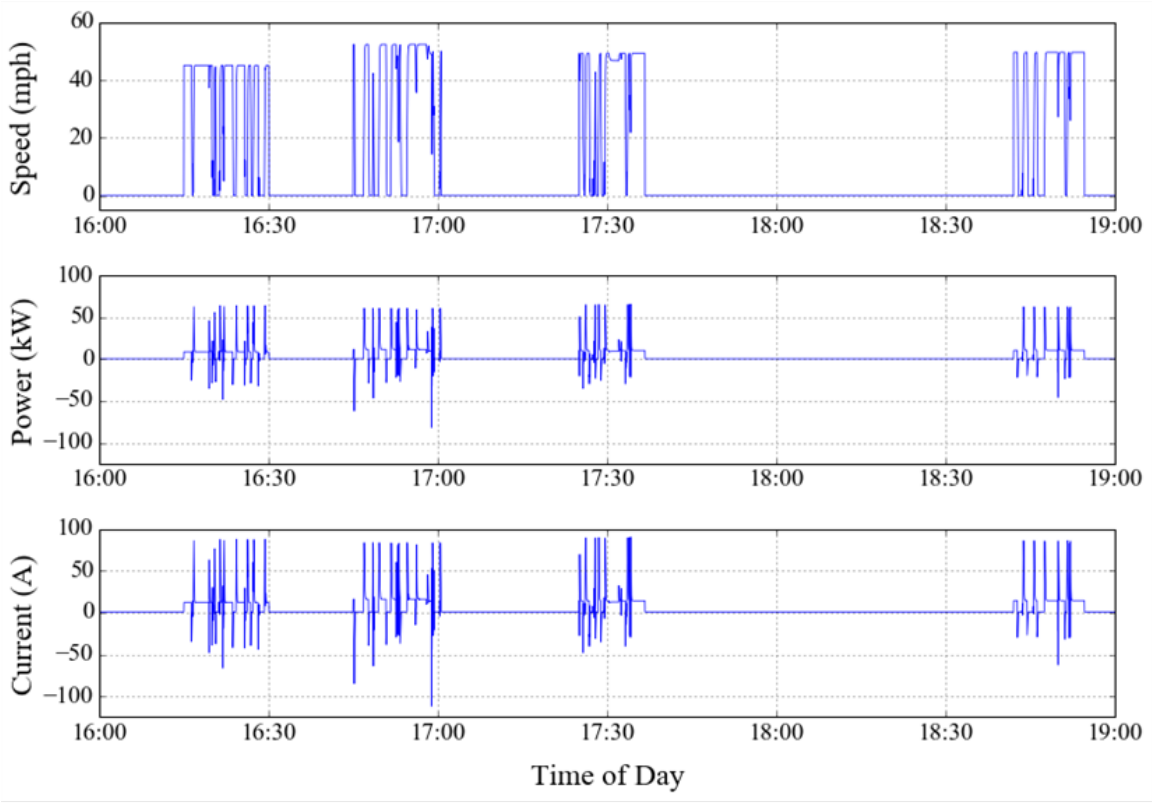

Figure 16 Speed profile of a sample vehicle and its corresponding battery power profile and current profile

4.1.2 Electric vehicle energy consumption model

EV energy consumption depends significantly on the microscopic speed profile data. There are several models and simulation tools available that can simulate EV energy consumptions based on the speed profile data. For example, ADVISOR (Markel et al., 2002; NREL, 2013) and Autonomie (Argonne National Laboratory, 2016) can simulate an EV's power profile, MPGe (mile per gasoline equivalent), state of charge (SOC) profile, etc. for any given speed profile. These tools simulate the detailed performance of the power train/propulsion systems, and hence are computationally expensive. This study uses the model proposed by Van Haaren (2012) as presented in Section 3.2.3.

4.1.3 Battery model

Battery degradation rate is different at different C-rates, so the current profile is needed to simulate battery life. The C-rate is a measure of the rate at which a battery is being discharged. It is defined as the discharge current divided by the theoretical current draw under which the battery would deliver its nominal rated capacity in one hour. A 1C discharge rate would deliver the battery's rated capacity in 1 hour. A 2C discharge rate implies that it will discharge twice as fast (30 minutes). Thus, battery current profile is required to compute battery degradation. In this study, an equivalent-circuit model for Li-ion battery is implemented as a Simulink block diagram to extract cell current profile using the power profile. The internal resistance and open-circuit voltage of the cell are implemented as 1-D lookup tables based on instantaneous battery state-of-charge. The equivalent-circuit model can be represented by equations (44)-(48). The definition of the parameters used are shown in Table 3.

$$V_{cell}\,(t) = V_{OC}\,(t) - I_{cell}\,(t) * R_{int}\,(t) \tag{44}$$

$$P_{cell}(t) = \frac{P_{batt}(t)}{N_{cell}} = V_{cell}(t) * I_{cell}(t) \tag{45}$$

$$V_{OC}(t) = f\big(E_{SOC}(t)\big) \tag{46}$$

$$R_{int}(t) = g\left(E_{SOC}(t)\right) \tag{47}$$

$$E_{SOC}(t) = E_{SOC}(0) + \frac{1}{B_{AhCap}} * \int_0^t \frac{I_{cell}(t)}{3600} dt \tag{48}$$

Table 3 Parameter definitions for equivalent-circuit battery model

Parameter	Definition
$\boldsymbol{V_{cell}(t)}$	Cell terminal voltage at time $\boldsymbol{t}$
$\boldsymbol{V_{OC}(t)}$	Cell open-circuit voltage at time $\boldsymbol{t}$
$\boldsymbol{I_{cell}(t)}$	Cell current at time $\boldsymbol{t}$
$\boldsymbol{R_{int}(t)}$	Cell internal resistance at time $\boldsymbol{t}$
$\boldsymbol{P_{cell}(t)}$	Electrical power out of the cell at time $\boldsymbol{t}$
$\boldsymbol{P_{batt}(t)}$	Electrical power out of the battery pack
$\boldsymbol{N_{cell}}$	Number of cells in the battery pack
$\boldsymbol{E_{SOC}(t)}$	State-of-charge at time $\boldsymbol{t}$
$\boldsymbol{f\left(\mathrm{E}_{SOC}(t)\right), g\left(E_{SOC}(t)\right)}$	1-D lookup tables as function of state-of-charge at time $\boldsymbol{t}$
$\boldsymbol{B_{AhCap}}$	Nominal ampere-hour capacity of the cell

4.1.4 Battery degradation model

Battery degradation causes capacity loss and impedance growth during operation and is also a result of storage. Operational degradation is called cycle aging, and storage degradation is called calendar aging. Calendar aging happens regardless of whether the battery is operated or not. It is mainly caused by the Li-ion loss during SEI formation at the graphite anode, and is strongly affected by two parameters: time and temperature (Wang et al., 2014). Cycle aging only happens when the battery is operating and there is current flow. The total battery energy capacity loss is the summation of these two effects.

This study uses a semi-empirical model developed by Wang et al. (2014) that includes three important experimental parameters: time, temperature, and discharge rate . They performed experiments for 1.5 Ah, 18650 cylindrical cells and created a test matrix to measure each cell. The cell has a $LiMn_{1/3}Ni_{1/3}Co_{1/3}$ + $LiMn_2O_4$ (NCM+LMO) cathode and a graphite anode. They modeled both calendar aging and cycle aging using substantial experimental data. The cycle aging model is for a given constant C-rate. In reality, it is not

possible for an EV to operate at a constant battery C-rate as the speed of the vehicle and hence, the power drawn from the battery changes with time. According to their results, under most conditions, the predicted values are within ±5% capacity loss of the measured values. The model is listed in equations (49)-(51).

$$Q_{loss,total} = Q_{loss,cycle} + Q_{loss,calendar} \quad (49)$$

$$Q_{loss,cycle} = (aT^2 + bT + c) \cdot exp[(dT + e) \cdot I_{rate}] \cdot Ah_{throughput} \quad (50)$$

$$Q_{loss,calendar} = f \cdot t^{0.5} \cdot exp(\frac{-E_a}{RT}) \quad (51)$$

Since the battery current and temperature changes with time, battery energy capacity loss caused by cycle aging and calendar aging are calculated every second. For each second, the current is assumed to be constant, and the instantaneous energy capacity loss $D_{Q_{loss,cycle}}$ can be expressed as the differential of $Q_{loss,cycle}$ with time t. Similarly, at variable temperature, capacity loss results from calendar aging can be expressed as the differential of $Q_{loss,calendar}$ with time t. The total energy capacity loss of cycle aging $\hat{Q}_{loss,cycle}$ and calendar aging $\hat{Q}_{loss,calendar}$ are computed by summing the respective losses for each second. Note that for constant temperature, $Q_{loss,calendar}$ and $\hat{Q}_{loss,calendar}$ are identical. The total battery energy capacity loss $Q_{loss,total}$ is the sum of cycle aging loss and calendar aging loss, which is updated every day until it is greater than 30%, criteria to retire battery from EV use. The equations (52)-(56) represents the model used in this study. The coefficient values and units are listed in Table 4.

$$D_{Q_{loss,cycle}} = (aT^2 + bT + c) \cdot exp[(dT + e) \cdot I_{rate}] \frac{dAh_{throughput}}{dt} \quad (52)$$

$$\hat{Q}_{loss,cycle} = \sum D_{Q_{loss,cycle}} \quad (53)$$

$$D_{Q_{loss,calendar}} = 0.5f \cdot exp(-\frac{E_a}{RT}) \cdot t^{-0.5} \quad (54)$$

$$\hat{Q}_{loss,calendar} = \sum D_{Q_{loss,calendar}} \quad (55)$$

$$Q_{loss,total} = \hat{Q}_{loss,cycle} + \hat{Q}_{loss,calendar} \quad (56)$$

Table 4 Coefficient values and units of the battery degradation model

Coefficient	Value and unit	Coefficient	Value and unit
$\boldsymbol{a}$	8.61E-6, 1/Ah-K^2	$\boldsymbol{I_{rate}}$	C-rate
$\boldsymbol{b}$	-5.125E-3, 1/Ah-K	$\boldsymbol{t}$	Days
$\boldsymbol{c}$	0.7629, 1/Ah	$\boldsymbol{E_a}$	24500, J/mole
$\boldsymbol{d}$	-6.7E-3, 1/K-(C-rate)	$\boldsymbol{R}$	8.314, J/(mole K)
$\boldsymbol{e}$	2.35, 1/(C-rate)	$\boldsymbol{T}$	Temperature (K)
$\boldsymbol{f}$	14876, 1/day$^{0.5}$		

4.1.5 Assumptions and simulation

In this study, one type of EV, similar to Nissan Leaf with 24 kWh Li-ion battery, is assumed to be used by all of the households. The battery is composed of 44 modules in parallel, where each module has 96 cells in serial, and each cell is 1.5 Ah and 3.75 V. The cell has a NCM+LMO cathode and a graphite anode. Because a NCM+LMO composite cathode presents a good balance of both energy density and power density (Fergus, 2010; Smith et al., 2011; Wang et al., 2014), it is considered as a promising candidate for vehicle applications.

The simulation of battery life in this study is based on the following assumptions. First, the battery is considered unusable in vehicle applications when it has depleted to 70% of its original energy storage capacity. Second, the degradation model is applied to the entire temperature range experienced in Indianapolis (monthly average temperature from -2.2ºC to 24.1ºC). Wang et al. performed experiments at 4 temperatures: 10ºC, 22ºC, 34ºC, 46ºC. This study assumes the model still applies at lower (but not extreme) temperatures. Third, this study assumes that EVs are only charged at home with a level 1 (120 V) or level 2 (240 V) charger. Thus, the effects of home charging on battery energy capacity loss can be ignored as level 1 and level 2 charging are both relatively slow. A 24 kWh EV battery takes about 12-13 hours for a full charge on a level 1 charger, and 7-8 hours on a level 2 charger (Morrow et al., 2008), which is equivalent to a 1/13 C-rate or 1/8 C-rate during charging. At such low C-rates, calendar aging is the dominant element that causes energy capacity loss. The energy capacity loss results from cycle aging at 1/8 C-rate at 20ºC for 8

hours is: 0.00066%, while the capacity loss results from calendar aging at 20ºC for first 8 hours is 0.37% for a new battery, and 0.0056% for a one-year battery. Since capacity loss due to calendar aging, equation (51), is a non-linear function of time, the calendar aging rate decreases with time, and becomes almost linear after one year. Most household vehicle daily trips are within 30 miles, and the energy consumption is less than half of the battery energy capacity and thus, most home charging events are less than 4 hours. Therefore, it is safe to ignore cycle aging effects on battery energy capacity loss during home charging. Fourth, when the EV is in use, regeneration during braking has the same effects on battery energy capacity loss as discharging at the same C-rate.

This study simulates 2306 household vehicle samples in Indianapolis. Each vehicle sample follows its unique travel pattern day by day. Five temperature scenarios are analyzed in this study: four constant temperature scenarios (10ºC, 15ºC, 20ºC and 25ºC) and one variable temperature scenario. The monthly average temperatures for Indianapolis are used in variable temperature scenario. Figure 17 shows the temperature profile of Indianapolis used in this study.

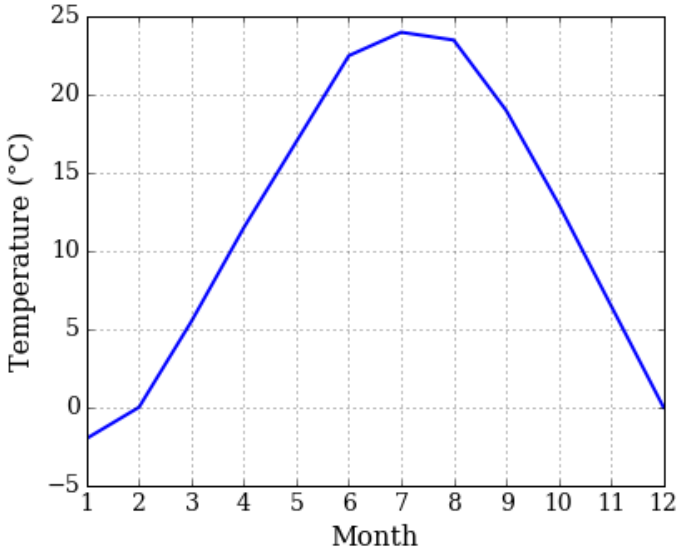

Figure 17 Indianapolis monthly average temperature

4.2 Results and discussion

The simulation results of EV battery lifespan for different temperature scenarios are presented and discussed in the following paragraphs. Each EV follows its unique speed profile every day. Some EVs may have up to 6 trips every day, while others may have only one trip per day. The impacts of temperature, vehicle travel patterns, and driving behavior are illustrated on battery life distribution to provide a holistic picture of battery lifespan for a large population of EVs.

Temperature affects both calendar aging and cycle aging. Figure 18(a) shows the simulated battery life histogram at four constant temperatures. The results indicate that the EV battery lifespan is (8.58±1.80) years at 10^{o}C, (7.33±0.73) years at 15^{o}C, (5.73±0.19) years at 20^{o}C, and (4.20±0.06) years at 25^{o}C. The EV battery life decreases as temperature increases. At higher temperatures, the battery degrades faster than at lower temperatures. The variation of EV battery life also decreases as temperature increases. This is because at higher temperatures, calendar aging dominates cycle aging as all EVs are at the same environmental temperature, and hence, the effects of vehicle travel patterns and driving behavior diminishes. In reality, temperature will not be constant all year long. The average monthly temperature profile in Indianapolis is used to simulate the EV battery lifespan in the city of Indianapolis. The annual average temperature in Indianapolis is 11.7^{o}C. The simulated EV battery lifespan is (7.54±1.68) years. Figure 18(b) shows the distribution of battery life in Indianapolis. Although the temperature profile of Indianapolis varies between -2.2^{o}C to 24.1^{o}C, the simulated result is similar to the scenario of 10^{o}C, and lies between the 10^{o}C and 15^{o}C scenarios (refer Figure 18(c)). Therefore, considering consistent vehicle travel patterns throughout the year, the average annual temperature is reasonable to use as an estimate in computing degradation due to temperature effects. Table 5 shows detailed percentile of battery lifespan and EV total travel distance for the five temperature scenarios.

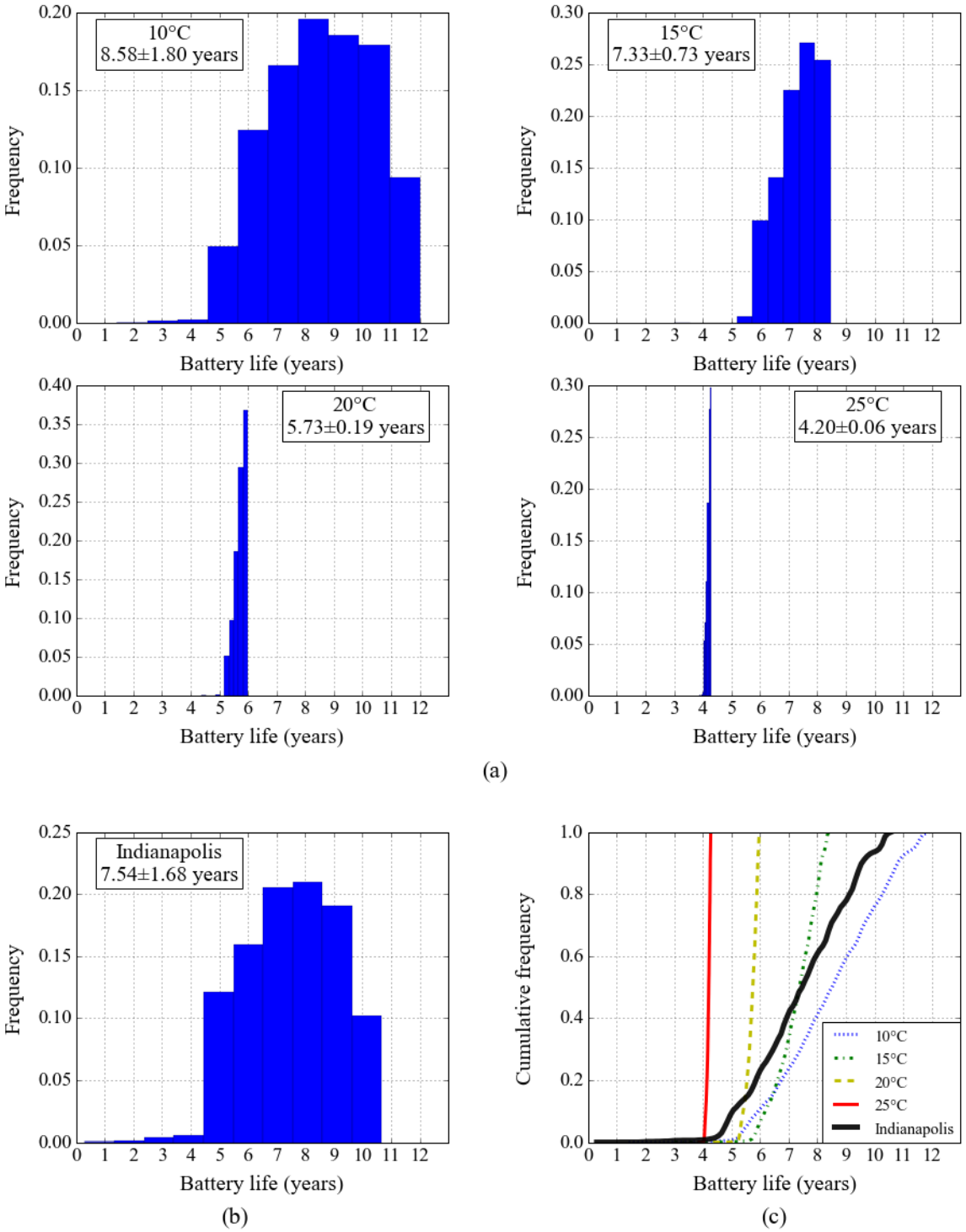

Figure 18 Battery lifespan distribution at: (a) constant temperatures; (b) Indianapolis temperature; (c) cumulative frequency curves for all scenarios

Table 5 The percentile of battery lifespan and total travel distances for different temperature scenarios

	Indianapolis		10ºC		15ºC		20ºC		25ºC	
	Value (years)	Value (miles)	Value (years)	Value (miles)	Value (years)	Value (miles)	Value (years)	Value (miles)	Value (years)	Value (miles)
0	0.30	1653	1.42	1845	3.01	1346	4.38	967	3.88	693
5	4.88	7612	5.62	8557	5.98	6128	5.34	4368	4.08	3126
10	5.15	14080	6.05	15937	6.23	11960	5.42	8676	4.11	6232
15	5.67	20522	6.52	23167	6.49	17738	5.51	12966	4.13	9336
20	5.96	24057	6.86	27517	6.66	21846	5.56	16210	4.15	11722
25	6.24	28160	7.20	32299	6.83	26037	5.61	19341	4.17	13968
30	6.57	33104	7.52	37529	6.98	29413	5.65	21909	4.18	15884
35	6.84	37303	7.79	42370	7.09	34320	5.68	25692	4.19	18600
40	7.03	41468	8.05	47277	7.21	39438	5.71	29845	4.20	21658
45	7.33	45874	8.34	52302	7.32	44586	5.74	34051	4.21	24739
50	7.57	50940	8.62	58141	7.44	49936	5.77	38548	4.22	28198
55	7.83	55766	8.89	63756	7.54	55476	5.79	43793	4.22	32193
60	8.04	59556	9.15	68126	7.63	60685	5.82	48672	4.23	35902
65	8.39	63527	9.51	72704	7.75	66484	5.84	53664	4.24	39676
70	8.57	68782	9.71	78730	7.82	72842	5.86	58531	4.24	43029
75	8.88	74111	10.04	85170	7.93	80160	5.88	65792	4.25	48768
80	9.23	79197	10.37	91204	8.03	88416	5.91	73454	4.26	54756
85	9.44	85882	10.64	98854	8.11	97524	5.92	81784	4.26	60833
90	9.65	94144	10.90	108763	8.18	111200	5.94	96430	4.27	73250
95	10.29	107729	11.49	124828	8.34	131553	5.97	116933	4.28	89239
100	10.68	146400	12.00	169360	8.46	177280	6.00	156720	4.28	119280

In order to gain insights into the relationship between vehicle travel patterns and battery lifespan, the simulated battery life is plotted against the total travel distance before the battery is depleted to 70% of its original capacity. Figure 19(a) shows battery lifespan versus total travel distance at four constant temperatures. The results illustrate that, at lower temperatures the effect of total travel distance is greater than that at higher temperatures. It means that at higher temperatures, battery lifespan is less sensitive to total travel distance. The negative slope indicates that as the EV travels longer, the battery life becomes shorter. The width of the strip shows the variation of battery life resulting from driving behavior such as average speed and speed deviation. As temperature increases, the strip starts

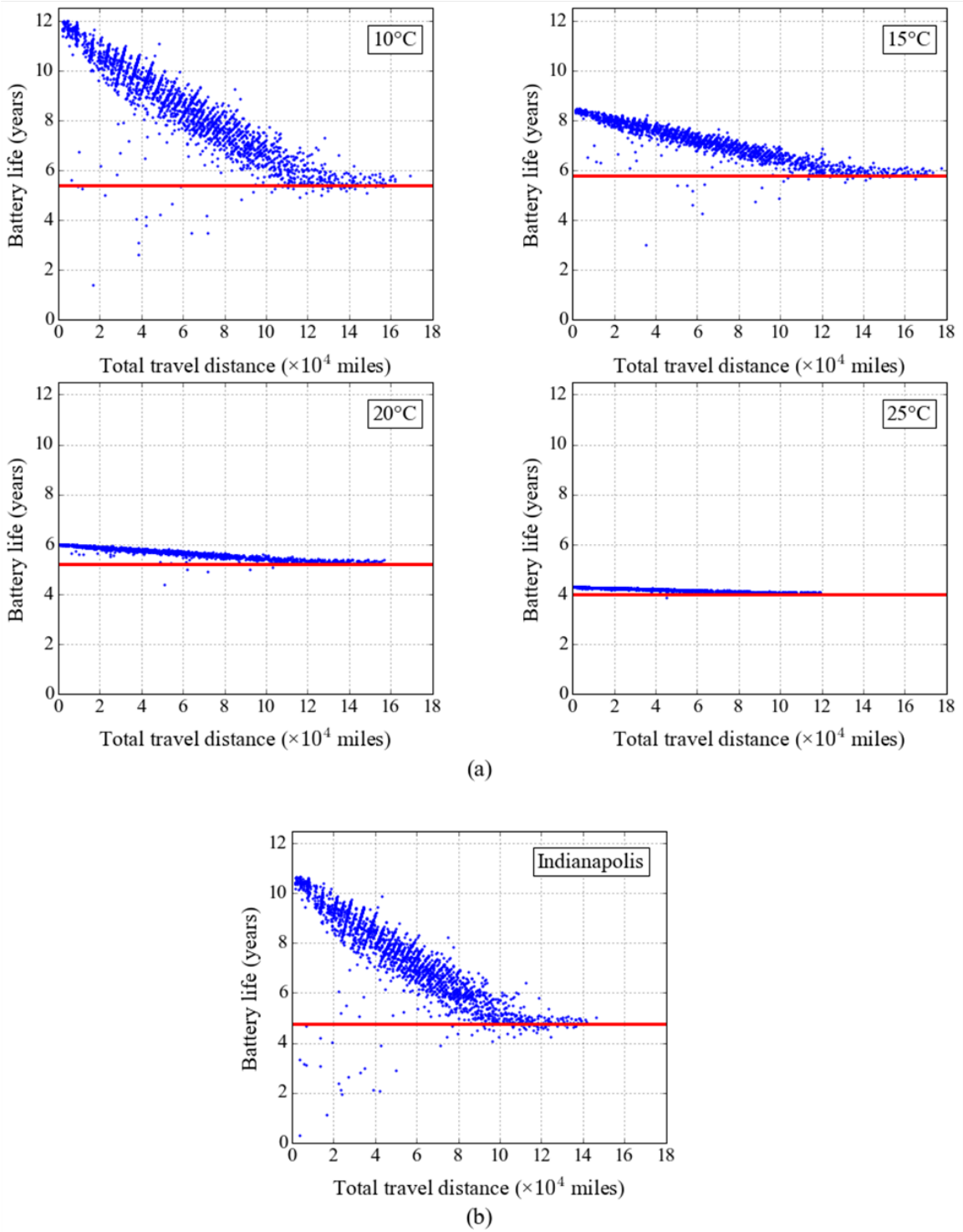

Figure 19 Impact of vehicle travel patterns on battery lifespan at: (a) constant temperatures; (b) Indianapolis temperature.

shrinking to almost a line, which indicates that the impact of driving behavior at lower temperature is greater than that at higher temperature. Another interesting finding is that after a certain point, the strip becomes almost horizontal, parallel to the x-axis. The horizontal red line provides intuitive information of minimum battery life under regular conditions, which is consistent with Table 5. Figure 19(b) shows the battery life versus total travel distance in Indianapolis. The results indicate that the impact of driving behavior in Indianapolis is similar to that of constant 10^{o}C, but the battery lifespan is less for similar total travel distance. The horizontal line intersects y-axis at about 4.8 years.

The impacts of driving behavior on battery lifespan are illustrated in Figure 20. Battery degradation due to cycle aging decreases as the average speed increases and speed deviation decreases. The average vehicle speed is higher and speed deviation is lower in uncongested traffic conditions. Though power consumption and C-rate are higher at higher constant speeds, at variable speeds, the magnitude of power losses/gains due to change in kinetic energy dominate those of the power losses at constant speed. Due to interactions between average speed and speed deviation, the variation in cycle aging is large.

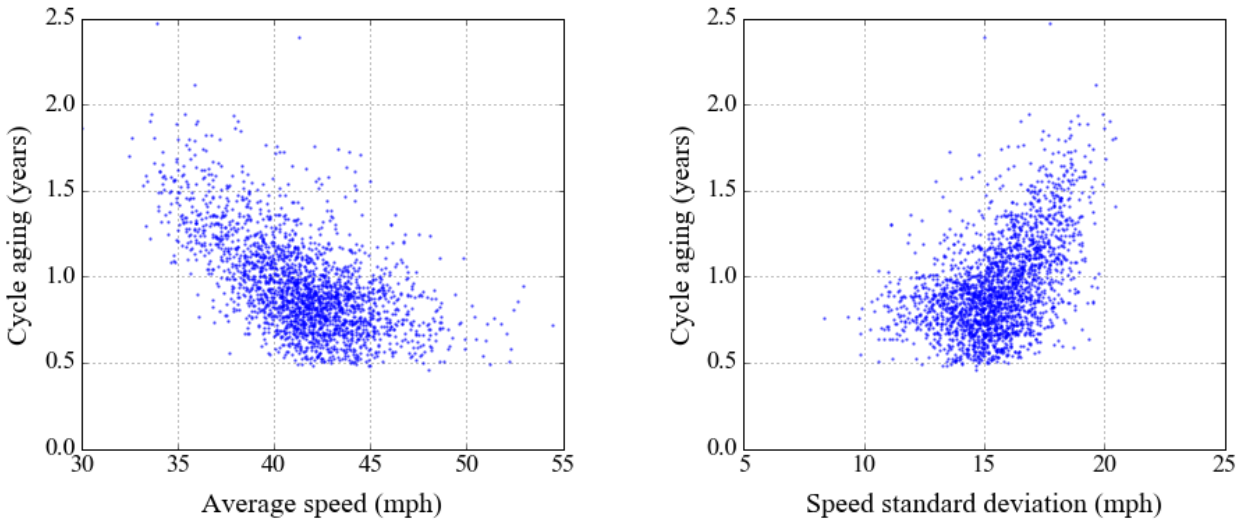

Figure 20 Impact of driving behavior on cycle aging for Indianapolis.

CHAPTER 5. CONCLUSIONS AND FUTURE WORK

This chapter summarizes the research, highlights its findings, and proposes directions for future research.

5.1 Summary

This study proposes two frameworks integrating modeling approaches used in transportation and energy sectors. First, the differences between the route choice behaviors of BEVs and ICEVs in a mixed traffic context with the potential for BEV range anxiety are analyzed, and their implications for traffic network performance under equilibrium conditions are examined. A multi-class DUE model is formulated and a microscopic simulation-based solution procedure is proposed. The use of microscopic simulation as part of the solution procedure enhance the accuracy of BEV energy consumption computation. Consequently, it aids in realistically capturing the effect of traffic congestion on BEV route selection. The traffic network performance, in terms of travel time and energy consumption, is analyzed with respect to the network characteristics (such as market penetration and traffic congestion) and factors that affect BEV route choice (such as electricity cost and range anxiety threshold). Second, the impacts of temperature, vehicle travel patterns, and driving behavior on EV battery lifespan are investigated. A multi-paradigm modeling framework integrated with microscopic traffic simulation model, EV energy consumption model, battery circuit model, and semi-empirical battery degradation model is developed. Realistic vehicle travel patterns are generated using real-world vehicle trips data from NHTS 2009 data, and simulated speed profiles for each trip using a microscopic traffic simulation model built for Indianapolis road network that reflect traffic conditions. An analytical EV energy consumption model and a semi-empirical battery degradation model are then employed to compute the battery lifespan under different temperature scenarios.

5.2 Major findings

First, the numerical analysis presented in CHAPTER 3 provides useful insights related to BEV route choice behavior and its impact on network performance. As battery SOC consumption for BEVs is lower at slower speeds, they can reduce their energy consumption by traveling on routes with slower speeds. Moreover, the RBS system equipped in BEVs reduces the rate of energy dissipation in stop-and-go traffic conditions and makes it more economical for them in terms of battery SOC consumption. The results from the numerical experiments indicate that BEVs choose routes with slower speeds, typically arterial routes, to reduce their battery SOC consumption and avoid range anxiety. Such potential unconventional route choice behavior by BEVs based on the generalized travel cost can decrease traffic congestion on routes with higher free flow speeds while increasing traffic congestion on routes with lower free flow speeds. This can lead to the improvement of traffic network performance and move the traffic network towards system optimal conditions in terms of travel time. Furthermore, with an increase in traffic congestion, BEV route choice behavior becomes similar to that of ICEVs as speeds in the network decrease, thereby reducing BEV incentive to switch routes to save on energy consumption. These insights can aid traffic operators to devise control strategies in the emerging mixed traffic stream, and policymakers to determine an optimal trajectory for promoting electric vehicles. Further, the insights related to energy consumption can aid energy operators to plan for infrastructure investments to support the increasing market penetration of electric vehicles.

Second, the multi-paradigm modeling framework presented in CHAPTER 4 is used to quantify the impacts of temperature, vehicle travel patterns, and driving behavior on EV battery lifespan that provide useful information for vehicle owners, policymakers and vehicle manufacturers. The results indicate that temperature has a substantial impact on battery lifespan, and can overshadow the impacts of vehicle travel patterns and driving behavior at high temperatures. The study insights aid vehicle owners to assess the lifetime cost of EV ownership, including maintenance cost, insurance cost and battery resale value,

based on their travel needs and geographic location. Since temperature has a significant impact on battery degradation, policymakers and vehicle manufacturers should consider regional temperature conditions while designing strategies like tax credits, battery warranty, etc., to promote EV adoption. Since the impacts of vehicle travel patterns and driving behavior are considerable at lower temperatures, these need to be factored in warranty strategies for colder regions. Vehicle manufacturers should factor the environmental conditions in which the battery will be used, as also vehicle travel patterns and consumer driving behaviors.

5.3 Future research directions

Future research should focus on developing optimal control strategies to enhance the network performance using the microscopic simulation-based solution procedure for the MCDUE model presented in this study. Also, statistical models based on real-world survey data should be developed to better understand the route choice preferences of EV drivers. Furthermore, the data presented in this study provides a realistic foundation for future work to study the dynamics of EV battery market, and provides insights for battery studies that will impact real-world battery lifespan. Future research should also target improving battery lifespan, and considering regional temperature profiles, vehicle travel patterns and EV driving behaviors.

REFERENCES

Adler, J.D., Mirchandani, P.B., 2014. Online routing and battery reservations for electric vehicles with swappable batteries. Transportation Research Part B: Methodological 70, 285–302.

Adler, J.D., Mirchandani, P.B., Xue, G., Xia, M., 2014. The electric vehicle shortest-walk problem with battery exchanges. Networks and Spatial Economics 1–19.

Argonne National Laboratory, 2016. Autonomie [WWW Document]. URL http://www.autonomie.net (accessed 1.30.16).

Artmeier, A., Haselmayr, J., Leucker, M., Sachenbacher, M., 2010. The shortest path problem revisited: Optimal routing for electric vehicles, in: KI 2010: Advances in Artificial Intelligence. Springer, pp. 309–316.

Astarita, V., 1996. A continuous time link model for dynamic network loading based on travel time function, in: Lesort, J.-B. (Ed.), Proceedings of the 13th International Symposium on Transportation and Traffic Theory. Pergamori, Oxford, pp. 79–102.

Aurbach, D., Zinigrad, E., Cohen, Y., Teller, H., 2002. A short review of failure mechanisms of lithium metal and lithiated graphite anodes in liquid electrolyte solutions. Solid State Ionics 148, 405–416. doi:10.1016/S0167-2738(02)00080-2

Ban, X.J., Liu, H.X., Ferris, M.C., Ran, B., 2008. A link-node complementarity model and solution algorithm for dynamic user equilibria with exact flow propagations. Transportation Research Part B: Methodological 42, 823–842.

Barceló, J., Casas, J., 2005. Dynamic network simulation with AIMSUN, in: Simulation Approaches in Transportation Analysis. Springer, pp. 57–98.

Becker, T.A., Sidhu, I., Tenderich, B., 2009. Electric vehicles in the United States: a new model with forecasts to 2030. Center for Entrepreneurship & Technology (CET). Technical Brief.

Blink, 2015. Car Charging Group, Inc. [ONLINE] Available at: http://www.blinknetwork.com.

Botsford, C., Szczepanek, A., 2009. Fast charging vs. slow charging: Pros and cons for the new age of electric vehicles, in: EVS24 International Battery, Hybrid Fuel Cell Electric Vehicle Symposium.

Broussely, M., Biensan, P., Bonhomme, F., Blanchard, P., Herreyre, S., Nechev, K., Staniewicz, R.J., 2005. Main aging mechanisms in Li ion batteries. Journal of Power Sources 146, 90–96. doi:10.1016/j.jpowsour.2005.03.172

Broussely, M., Herreyre, S., Biensan, P., Kasztejna, P., Nechev, K., Staniewicz, R.J., 2001. Aging mechanism in Li ion cells and calendar life predictions. Journal of Power Sources 97–98, 13–21. doi:10.1016/S0378-7753(01)00722-4

Casas, J., Ferrer, J.L., Garcia, D., Perarnau, J., Torday, A., 2010. Traffic simulation with aimsun, in: Fundamentals of Traffic Simulation. Springer, pp. 173–232.

Chabini, I., 1998. Discrete dynamic shortest path problems in transportation applications: Complexity and algorithms with optimal run time. Transportation Research Record: Journal of the Transportation Research Board 170–175.

Chan, H.L., 2000. A new battery model for use with battery energy storage systems and electric vehicles power systems, in: Power Engineering Society Winter Meeting, 2000. IEEE. pp. 470–475.

Chen, T.D., Kockelman, K.M., Khan, M., others, 2013. The electric vehicle charging station location problem: a parking-based assignment method for Seattle, in: Transportation Research Board 92nd Annual Meeting. pp. 13–1254.

Clarke, P., Muneer, T., Cullinane, K., 2010. Cutting vehicle emissions with regenerative braking. Transportation Research Part D: Transport and Environment 15, 160–167. doi:10.1016/j.trd.2009.11.002

CPLEX, I.I., 2012. V12. 5: User's manual for CPLEX.

DeMuro, D., 2013. 2013 Nissan Leaf gets new battery warranty [WWW Document]. Autotrader. URL http://www.autotrader.com/car-news/2013-nissan-leaf-gets-new-battery-warranty-201645 (accessed 7.12.14).

EPRI, 2007. Environmental assessment of plug-in hybrid electric vehicles. Technical Report 1015325, Electric Power Research Institute 1, 1–38.

Federal Highway Administration, 2010. National Household Travel Survey of 2009, [ONLINE] Available at: http://nhts.ornl.gov.

Fergus, J.W., 2010. Recent developments in cathode materials for lithium ion batteries. Journal of Power Sources 195, 939–954. doi:10.1016/j.jpowsour.2009.08.089

Funk, K., Rabl, A., 1999. Electric versus conventional vehicles: social costs and benefits in France. Transportation Research Part D: Transport and Environment 4, 397–411.

Guenther, C., Schott, B., Hennings, W., Waldowski, P., Danzer, M.A., 2013. Model-based investigation of electric vehicle battery aging by means of vehicle-to-grid scenario simulations. Journal of Power Sources 239, 604–610. doi:10.1016/j.jpowsour.2013.02.041

He, F., Wu, D., Yin, Y., Guan, Y., 2013. Optimal deployment of public charging stations for plug-in hybrid electric vehicles. Transportation Research Part B: Methodological 47, 87–101.

He, F., Yin, Y., Lawphongpanich, S., 2014. Network equilibrium models with battery electric vehicles. Transportation Research Part B: Methodological 67, 306–319.

Hess, A., Malandrino, F., Reinhardt, M.B., Casetti, C., Hummel, K.A., Barceló-Ordinas, J.M., 2012. Optimal deployment of charging stations for electric vehicular networks, in: Proceedings of the First Workshop on Urban Networking. pp. 1–6.

Huang, S., Safiullah, H., Xiao, J., Hodge, B.M.S., Hoffman, R., Soller, J., Jones, D., Dininger, D., Tyner, W.E., Liu, A., Pekny, J.F., 2012. The effects of electric vehicles on residential households in the city of Indianapolis. Energy Policy 49, 442–455. doi:10.1016/j.enpol.2012.06.039

Ichimori, T., Ishii, H., Nishida, T., 1983. Two routing problems with the limitation of fuel. Discrete Applied Mathematics 6, 85–89.

Jiang, N., Xie, C., 2014. Computing and analyzing mixed equilibrium network flows with gasoline and electric vehicles. Computer-Aided Civil and Infrastructure Engineering 29, 626–641.

Jiang, N., Xie, C., Waller, S., 2012. Path-constrained traffic assignment: model and algorithm. Transportation Research Record: Journal of the Transportation Research

Board 25–33.

Johnson, V.H., 2002. Battery performance models in ADVISOR. Journal of power sources 110, 321–329.

Kang, J.E., Recker, W.W., 2009. An activity-based assessment of the potential impacts of plug-in hybrid electric vehicles on energy and emissions using 1-day travel data. Transportation Research Part D: Transport and Environment 14, 541–556. doi:10.1016/j.trd.2009.07.012

Kuby, M., Lim, S., 2005. The flow-refueling location problem for alternative-fuel vehicles. Socio-Economic Planning Sciences 39, 125–145.

Lee, Y.J., Choi, H.Y., Ha, C.W., Yu, J.H., Hwang, M.J., Doh, C.H., Choi, J.H., 2015. Cycle life modeling and the capacity fading mechanisms in a graphite/LiNi<inf>0.6</inf>Co<inf>0.2</inf>Mn<inf>0.2</inf>O<inf>2</inf> cell. Journal of Applied Electrochemistry 45, 419–426. doi:10.1007/s10800-015-0811-6

Lin, Z., Greene, D., 2011. Promoting the market for plug-in hybrid and battery electric vehicles. Transportation Research Record: Journal of the Transportation Research Board 2252, 49–56. doi:10.3141/2252-07

Maia, R., Silva, M., Araújo, R., Nunes, U., 2011. Electric vehicle simulator for energy consumption studies in electric mobility systems, in: Integrated and Sustainable Transportation System (FISTS), 2011 IEEE Forum on. pp. 227–232.

Mak, H.-Y., Rong, Y., Shen, Z.-J.M., 2013. Infrastructure planning for electric vehicles with battery swapping. Management Science 59, 1557–1575.

Marano, V., Onori, S., Guezennec, Y., Rizzoni, G., Madella, N., 2009. Lithium-ion batteries life estimation for plug-in hybrid electric vehicles. Vehicle Power and Propulsion Conference, 2009. VPPC ’09. IEEE 536–543. doi:10.1109/VPPC.2009.5289803

Markel, T., Brooker, A., Hendricks, T., Johnson, V., Kelly, K., Kramer, B., O’Keefe, M., Sprik, S., Wipke, K., 2002. ADVISOR: A systems analysis tool for advanced vehicle modeling. Journal of Power Sources 110, 255–266. doi:10.1016/S0378-7753(02)00189-1

Miralinaghi, M., Keskin, B.B., Lou, Y., Roshandeh, A.M., 2016. Capacitated Refueling Station Location Problem with Traffic Deviations Over Multiple Time Periods. Networks and Spatial Economics 1–23. doi:10.1007/s11067-016-9320-3

Miralinaghi, M., Lou, Y., Keskin, B.B., Zarrinmehr, A., Shabanpour, R., 2017. Refueling Station Location Problem with Traffic Deviation Considering Route Choice and Demand Uncertainty. International Journal of Hydrogen Energy 42, 3335–3351. doi:10.1016/j.ijhydene.2016.12.137

Mock, P., Schmid, S.A., Friedrich, H.E., 2010. Market prospects of electric passenger vehicles. Electric and Hybrid Vehicles: Power Sources, Models, Sustainability, Infrastructure and the Market. Elsevier.

Mock, P., Yang, Z., 2014. Driving electrification: A global comparison of fiscal incentive policy for electric vehicles. The International Council on Clean Transportation (ICCT) 22, 2014.

Morrow, K., Karner, D., Francfort, J., 2008. Plug-in hybrid electric vehicle charging infrastructure review. US Department of Energy-Vehicle Technologies Program 34. doi:10.2172/946853

Neubauer, J., Brooker, A., Wood, E., 2012. Sensitivity of battery electric vehicle economics to drive patterns, vehicle range, and charge strategies. Journal of Power Sources 209, 269–277. doi:10.1016/j.jpowsour.2012.02.107

Neubauer, J., Pesaran, A., 2011. The ability of battery second use strategies to impact plug-in electric vehicle prices and serve utility energy storage applications. Journal of Power Sources 196, 10351–10358. doi:10.1016/j.jpowsour.2011.06.053

Nie, Y.M., Ghamami, M., 2013. A corridor-centric approach to planning electric vehicle charging infrastructure. Transportation Research Part B: Methodological 57, 172–190.

NREL, 2013. ADVISOR Advanced Vehicle Simulator. [ONLINE] Available at: http://adv-vehicle-sim.sourceforge.net.

Pearre, N.S., Kempton, W., Guensler, R.L., Elango, V. V., 2011. Electric vehicles: How much range is required for a day's driving? Transportation Research Part C: Emerging

Technologies 19, 1171–1184. doi:10.1016/j.trc.2010.12.010

Peeta, S., Ziliaskopoulos, A.K., 2001. Foundations of Dynamic Traffic Assignment: The Past, the Present and the Future. Networks and Spatial Economics 1, 233–265. doi:10.1023/A:1012827724856

Plett, G.L., 2004. Extended Kalman filtering for battery management systems of LiPB-based HEV battery packs: Part 3. State and parameter estimation. Journal of power sources 134, 277–292.

Purewal, J., Wang, J., Graetz, J., Soukiazian, S., Tataria, H., Verbrugge, M.W., 2014. Degradation of lithium ion batteries employing graphite negatives and nickel-cobalt-manganese oxide + spinel manganese oxide positives: Part 2, chemical-mechanical degradation model. Journal of Power Sources 272, 1154–1161. doi:10.1016/j.jpowsour.2014.07.028

Rezvani, Z., Jansson, J., Bodin, J., 2015. Advances in consumer electric vehicle adoption research: A review and research agenda. Transportation Research Part D: Transport and Environment 34, 122–136. doi:10.1016/j.trd.2014.10.010

Rezvanizaniani, S.M., Liu, Z., Chen, Y., Lee, J., 2014. Review and recent advances in battery health monitoring and prognostics technologies for electric vehicle (EV) safety and mobility. Journal of Power Sources 256, 110–124.

Sachenbacher, M., Leucker, M., Artmeier, A., Haselmayr, J., 2011. Efficient energy-optimal routing for electric vehicles, in: AAAI.

Saxena, S., Le Floch, C., Macdonald, J., Moura, S., 2015. Quantifying EV battery end-of-life through analysis of travel needs with vehicle powertrain models. Journal of Power Sources 282, 265–276. doi:10.1016/j.jpowsour.2015.01.072

Schneider, M., Stenger, A., Goeke, D., 2014. The electric vehicle-routing problem with time windows and recharging stations. Transportation Science 48, 500–520.

Senart, A., Kurth, S., Le Roux, G., 2010. Assessment framework of plug-in electric vehicles strategies, in: Smart Grid Communications (SmartGridComm), 2010 First IEEE International Conference on. pp. 155–160.

Shepherd, S., Bonsall, P., Harrison, G., 2012. Factors affecting future demand for electric

vehicles: A model based study. Transport Policy 20, 62–74.

Smith, a. J., Burns, J.C., Xiong, D., Dahn, J.R., 2011. Interpreting high precision coulometry results on Li-ion cells. Journal of The Electrochemical Society 158, A1136. doi:10.1149/1.3625232

Smith, M.J., 1984. The stability of a dynamic model of traffic assignment-an application of a method of Lyapunov. Transportation Science 18, 245–252.

Storandt, S., 2012. Quick and energy-efficient routes: computing constrained shortest paths for electric vehicles, in: Proceedings of the 5th ACM SIGSPATIAL International Workshop on Computational Transportation Science. pp. 20–25.

Straubel, J.B., 2008. Roadster efficiency and range [WWW Document]. Tesla Motors. URL https://www.teslamotors.com/blog/roadster-efficiency-and-range (accessed 7.12.14).

Tanaka, D., Ashida, T., Minami, S., 2008. An analytical method of EV velocity profile determination from the power consumption of electric vehicles, in: Vehicle Power and Propulsion Conference, 2008. VPPC'08. IEEE. pp. 1–3.

Tate, E.D., Harpster, M.O., Savagian, P.J., 2008. The electrification of the automobile: from conventional hybrid, to plug-in hybrids, to extended-range electric vehicles. SAE international journal of passenger cars-electronic and electrical systems 1, 156–166.

Thomas, E. V., Bloom, I., Christophersen, J.P., Battaglia, V.S., 2008. Statistical methodology for predicting the life of lithium-ion cells via accelerated degradation testing. Journal of Power Sources 184, 312–317. doi:10.1016/j.jpowsour.2008.06.017

U.S. EIA, 2012. Annual Energy Review 2011, U.S. Energy Information Administration. doi:/EIA-1384(2011)

U.S. EPA, 2015. Inventory of U.S. greenhouse gas emissions and sinks: 1990-2013. U.S. Environmental Protection Agency 564. doi:EPA 430-R-13-001

Upchurch, C., Kuby, M., Lim, S., 2009. A model for location of capacitated alternative-fuel stations. Geographical Analysis 41, 85–106.

USDOE, 2016. All-electric vehicles. [ONLINE] Available at:

http://www.fueleconomy.gov/feg/evtech.shtml.

USDOE, 2014. Benefits and considerations of electricity as a vehicle fuel. [ONLINE] Available at: http://www.afdc.energy.gov/fuels/electricity_benefits.html.

Van Haaren, R., 2012. Assessment of electric cars ' range requirements and usage patterns based on driving behavior recorded in the National Household Travel Survey of 2009, Earth and Environmental Engineering Department, Columbia University, Fu Foundation School of Engineering and Applied Science, New York.

Vetter, J., Novak, P., Wagner, M.R., Veit, C., Moller, K.C., Besenhard, J.O., Winter, M., Wohlfahrt-Mehrens, M., Vogler, C., Hammouche, A., 2005. Ageing mechanisms in lithium-ion batteries. Journal of Power Sources 147, 269–281. doi:10.1016/j.jpowsour.2005.01.006

Wang, J., Liu, P., Hicks-Garner, J., Sherman, E., Soukiazian, S., Verbrugge, M., Tataria, H., Musser, J., Finamore, P., 2011. Cycle-life model for graphite-LiFePO4 cells. Journal of Power Sources 196, 3942–3948. doi:10.1016/j.jpowsour.2010.11.134

Wang, J., Purewal, J., Liu, P., Hicks-Garner, J., Soukazian, S., Sherman, E., Sorenson, A., Vu, L., Tataria, H., Verbrugge, M.W., 2014. Degradation of lithium ion batteries employing graphite negatives and nickel-cobalt-manganese oxide + spinel manganese oxide positives: Part 1, aging mechanisms and life estimation. Journal of Power Sources 269, 937–948.

Wang, M., 1999. Fuel-cycle greenhouse gas emissions impacts of alternative transportation fuels and advanced vehicle technologies. Transportation Research Record 1664, 9. doi:10.3141/1664-02

Wang, Y.-W., Lin, C.-C., 2009. Locating road-vehicle refueling stations. Transportation Research Part E: Logistics and Transportation Review 45, 821–829.

Weiller, C., 2011. Plug-in hybrid electric vehicle impacts on hourly electricity demand in the United States. Energy Policy 39, 3766–3778. doi:10.1016/j.enpol.2011.04.005

Wipke, K.B., Cuddy, M.R., Burch, S.D., 1999. ADVISOR 2.1: A user-friendly advanced powertrain simulation using a combined backward/forward approach. Vehicular Technology, IEEE Transactions on 48, 1751–1761.

Wood, E., Alexander, M., Bradley, T.H., 2011. Investigation of battery end-of-life conditions for plug-in hybrid electric vehicles. Journal of Power Sources 196, 5147–5154. doi:10.1016/j.jpowsour.2011.02.025

Wright, R.B., Motloch, C.G., Belt, J.R., Christophersen, J.P., Ho, C.D., Richardson, R.A., Bloom, I., Jones, S.A., Battaglia, V.S., Henriksen, G.L., Unkelhaeuser, T., Ingersoll, D., Case, H.L., Rogers, S.A., Sutula, R.A., 2002. Calendar- and cycle-life studies of advanced technology development program generation 1 lithium-ion batteries. Journal of Power Sources 110, 445–470. doi:10.1016/S0378-7753(02)00210-0

Wu, X., Freese, D., Cabrera, A., Kitch, W.A., 2015. Electric vehicles' energy consumption measurement and estimation. Transportation Research Part D: Transport and Environment 34, 52–67.

Xi, X., Sioshansi, R., Marano, V., 2013. Simulation-optimization model for location of a public electric vehicle charging infrastructure. Transportation Research Part D: Transport and Environment 22, 60–69. doi:10.1016/j.trd.2013.02.014

Yao, E., Wang, M., Song, Y., Yang, Y., 2013. State of charge estimation based on microscopic driving parameters for electric vehicle's battery. Mathematical Problems in Engineering 2013.

Yu, A.S.O., Silva, L.L.C., Chu, C.L., Nascimento, P.T.S., Camargo Jr, A.S., 2011. Electric vehicles: struggles in creating a market, in: Technology Management in the Energy Smart World (PICMET), 2011 Proceedings of PICMET'11: pp. 1–13.

Contacts

For more information:

Srinivas Peeta
Principal Investigator
Professor of Civil Engineering & Director
NEXTRANS Center, Purdue University
Ph: (765) 496 9726
Fax: (765) 807 3123
peeta@purdue.edu
https://engineering.purdue.edu/~peeta/

NEXTRANS Center
Purdue University - Discovery Park
3000 Kent Ave.
West Lafayette, IN 47906

nextrans@purdue.edu
(765) 496-9724

www.purdue.edu/dp/nextrans